Investigation of Factors Affecting Collision CVD Estimation and the Impact of Decomposition Errors on the EMG Signal Coherence

by

Srivatsa Subba Rao Majeti

Submitted in partial fulfillment of the requirements
for the degree of Master of Applied Science

at

Dalhousie University
Halifax, Nova Scotia
July 2010

DALHOUSIE UNIVERSITY

DEPARTMENT OF ELECTRICAL AND COMPUTER ENGINEERING

The undersigned hereby certify that they have read and recommend to the Faculty of Graduate Studies for acceptance a thesis entitled "Investigation of Factors Affecting Collision CVD Estimation and the Impact of Decomposition Errors on the EMG Signal Coherence" by Srivatsa Subba Rao Majeti in partial fulfilment of the requirements for the degree of Master of Applied Science.

Dated: July 20, 2010

Supervisor: _____

Readers: _____

_____

_____

DALHOUSIE UNIVERSITY

DATE: July 20, 2010

AUTHOR: Srivatsa Subba Rao Majeti

TITLE: Investigation of Factors Affecting Collision CVD Estimation and the Impact of Decomposition Errors on the EMG Signal Coherence

DEPARTMENT OR SCHOOL: Department of Electrical & Computer Engineering

DEGREE: MASc CONVOCATION: May YEAR: 2011

Permission is herewith granted to Dalhousie University to circulate and to have copied for non-commercial purposes, at its discretion, the above title upon the request of individuals or institutions.

_____

Signature of Author

Dedication

To my beloved Master and family

To them I dedicate this thesis

TABLE OF CONTENTS

LIST OF TABLES

LIST OF FIGURES

ABSTRACT

Experimental measurements are never perfect, even with sophisticated modern instruments. One of the fundamental problems in signal measurement is distinguishing the noise from the signal. Sometimes the two can be partly distinguished on the basis of frequency components: for example, the signal may contain mostly low-frequency components and the noise may be located at higher frequencies. This is the basis of filtering.

This thesis discusses some changes in the experimental protocol such as determining a suitable stimulation site to elicit full compound nerve action potentials (CNAP). The effect of sampling frequency and smoothing techniques to improve the resolution of the conduction velocity distribution (CVD) estimates will also be discussed. A change in stimulation site to elicit the full CNAPs is proposed after realizing that it is relatively difficult to stimulate at the same location to recruit the nerve fibers repeatedly at the elbow. Thus, the stimulation site was changed from elbow to wrist to elicit the full CNAPs. From the simulations it is evident that there was some signal information beyond 2.5 kHz frequency resulting in an increase in the sampling rate from 5 kHz to 10 kHz. The results obtained after employing smoothing techniques improved the CVD resolution. The simulation results were corroborated with the experimental results obtained.

Another aspect of this thesis is to check the error tolerance of the EMG decomposition algorithm. Once the muscle electrical activity is recorded, MU trains undergo an automatic decomposition process. Decomposition errors are present in most contractions, thus a human operator has to make changes/correct the values of the motor unit firing times.

From the data acquired, false negatives, false positives and false negative-positive errors have been introduced. Different levels of errors to measure the coherence between two motor-unit firing trains from a muscle contraction were also introduced. The firing rate curves are computed for each MU to analyze the interactions between two motor units (MU). The false negatives type of errors was found to be least detrimental. Whereas the false positives and false negative-positive errors affected coherence the most, their error tolerance was only a single error per 5 seconds.

LIST OF ABBREVIATIONS

ANNs	Artificial Neural Networks
CIS	Common Input Strength
CD	Common Drive
CTS	Carpal Tunnel Syndrome
CVD	Conduction velocity distribution
CNAP	Compound nerve action potential
EMG	Electromyography
FN	False negatives
FP	False positives
FNP	False negative-positive
ISI	Inter Stimulus Interval
ISI	Inter Spike Interval
IFI	Inter Firing Interval
MU	Motor Unit
MUAP	Motor unit action potential
MUAPT	Motor unit action potential train
MVC	Maximal Voluntary Contraction
MSE	Mean Square Error
NCS	Nerve conduction studies
PMSE	Percent mean square error

ACKNOWLEDGMENTS

This research work would not have been possible without the support of many people. First, I am extremely thankful to my supervisor, Dr. Jose Gonzalez-Cueto, for his supervision, support, guidance, and encouragement throughout the duration of this work.

I would like to thank my supervisory committee members Dr. Jason Gu and Dr. Cheryl Kozey for taking part in the thesis and reviewing it. I would also like to express my gratitude to Dr. Zeynep Erim who provided me with the EMG data required to conduct the coherence analysis.

I would like to thank all of my friends, colleagues and staff at Dalhousie University for sharing many thoughts, experiences, and good times. Also, I wish to express my sincere love to my beloved ones my brothers, my sisters, my cousins and my nephews for their unconditional love, support and encouragement.

Finally, and most importantly, I wish to thank my master and parents for their love and support throughout my studies abroad, to them I dedicate this thesis.

CHAPTER 1 Introduction

1.1 Nerve conduction studies

Nerve conduction studies are done to assess the damage to the peripheral nervous system which includes all the nerves that lead away from the brain and spinal cord and the smaller nerves that branch out from those nerves. Nerve conduction studies are often used to help determine the presence of carpal tunnel syndrome.

The carpal tunnel is the site where the median nerve is most commonly entrapped. The carpal tunnel is a cavity formed in the wrist bones through which the carpal ligament, nine flexor tendons and the median nerve pass. Abnormalities in the carpal tunnel, such as bone spurs and fractures and/or inflammation of the ligament, tendons or the median nerve can cause the median nerve to be entrapped. Carpal Tunnel Syndrome (CTS) occurs when the median nerve becomes entrapped in the carpal tunnel.

The causes of CTS may include repetitive use of wrist, various injuries, including previous fractures of the wrist. The general symptoms of CTS are numbness, tingling, or burning sensations in the thumb and fingers, particularly the index and middle fingers, which are affected by the median nerve, pain in the hands or wrists, loss of dexterity or gripping strength.

1.2 How is the diagnosis made?

A careful examination of the affected hand and wrist is performed after a detailed history of the patient is taken. The physician examines the hands, wrists, elbows, and shoulders to check for nerve compression or other problems, and may perform a more detailed examination to look for medical conditions. The examination includes:

- Tapping the wrist over the median nerve to see if this reproduces the symptoms (the Tinel test)
- Gently holding the wrist bent forward for 30 to 60 seconds to see if this reproduces the symptoms (the Phalen test)
- Gently using pinpricks and light stroking motions with a pin to see if any part of the hand has lost sensitivity (a sign of nerve damage)

1.3 Assessment based on Nerve Conduction Study

In the nerve conduction test, several flat metal disc electrodes are attached to the skin over the elbow and the wrist sites with tape. The stimulating electrodes are placed directly over the nerve and a recording ring electrode is placed over the index finger under control of that nerve. Several quick electrical pulses are given to the nerve and the response of the electrical pulse is recorded.

The median nerve is stimulated at the wrist 12cm proximal to the recording site and a sensory action potential is antidromically recorded. An average sensory conduction

velocity of 45m/s or less indicates the presence of CTS [1, 2]. Distal latency is defined as the time taken by the nerve action potential to travel from the stimulation site to the recording site. Conduction velocity is given by the distance between stimulating and recording electrode divided by the distal latency [3]. The Conduction velocity distribution estimation using the collision technique is used as part of the study in this thesis. The collision technique can be used to selectively activate nerve fibers of different diameters by varying the delay between two stimuli - a distal supramaximal stimulus and a delayed proximal stimulus [4].

It is also believed that certain factors like age and sex can give a false positive result for median nerve neuropathy. The upper limit of the normal latency cut-off varies according to these factors.

1.4 Introduction to EMG

Electromyography (EMG) is the investigation of muscle activity through electrical signals from muscles to diagnose neuromuscular disorders. EMG focuses on characterizing motor unit action potentials (MUAP) during muscle contractions. A motor unit (MU) activates the muscle fibers, a contraction occur with active participation of several MUs. A brief introduction to the anatomy of the MU and the decomposition of the EMG signal is provided in the following section.

1.5 MU anatomy, Activation and Recording

The anatomical concept most relevant to understanding the electrical activity of

muscle is Liddell and Sherrington's motor unit [5]. The motor unit consists of an anterior horn cell, its axon, and terminal branches (all of which make up the motor neuron), the neuromuscular junction, and all the individual muscle fibers it innervates. The size of the motor unit, that is the number of muscle fibers innervated by a single anterior horn cell, varies with each muscle.

In routine needle-electrode examination (ie, EMG) of voluntary muscle contraction, the electro - diagnostic consultant assesses the signature electrical signal generated by the MUs, termed the MUAP. MU recruitment is defined as the successive activation of the same and additional MUs with increasing strength of voluntary muscle contraction [6]. MU recruitment results in a strong efficient muscle contraction. Patterns of recruitment may differ between various types of motor activation. The myoelectric or EMG signal is amplified by using a high-quality differential amplifier and then displayed on a digital screen (usually a computer monitor).

EMG signals are made up of superimposed MUAPs from several motor units. The measured EMG signals can be decomposed into their constituent MUAPs. MUAPs from different motor units tend to have different characteristic shapes, while MUAPs recorded by the same electrode from the same motor unit are typically similar. Figure 1 presents a pictorial outline of the decomposition of the surface EMG signal into its constituent motor unit action potentials.

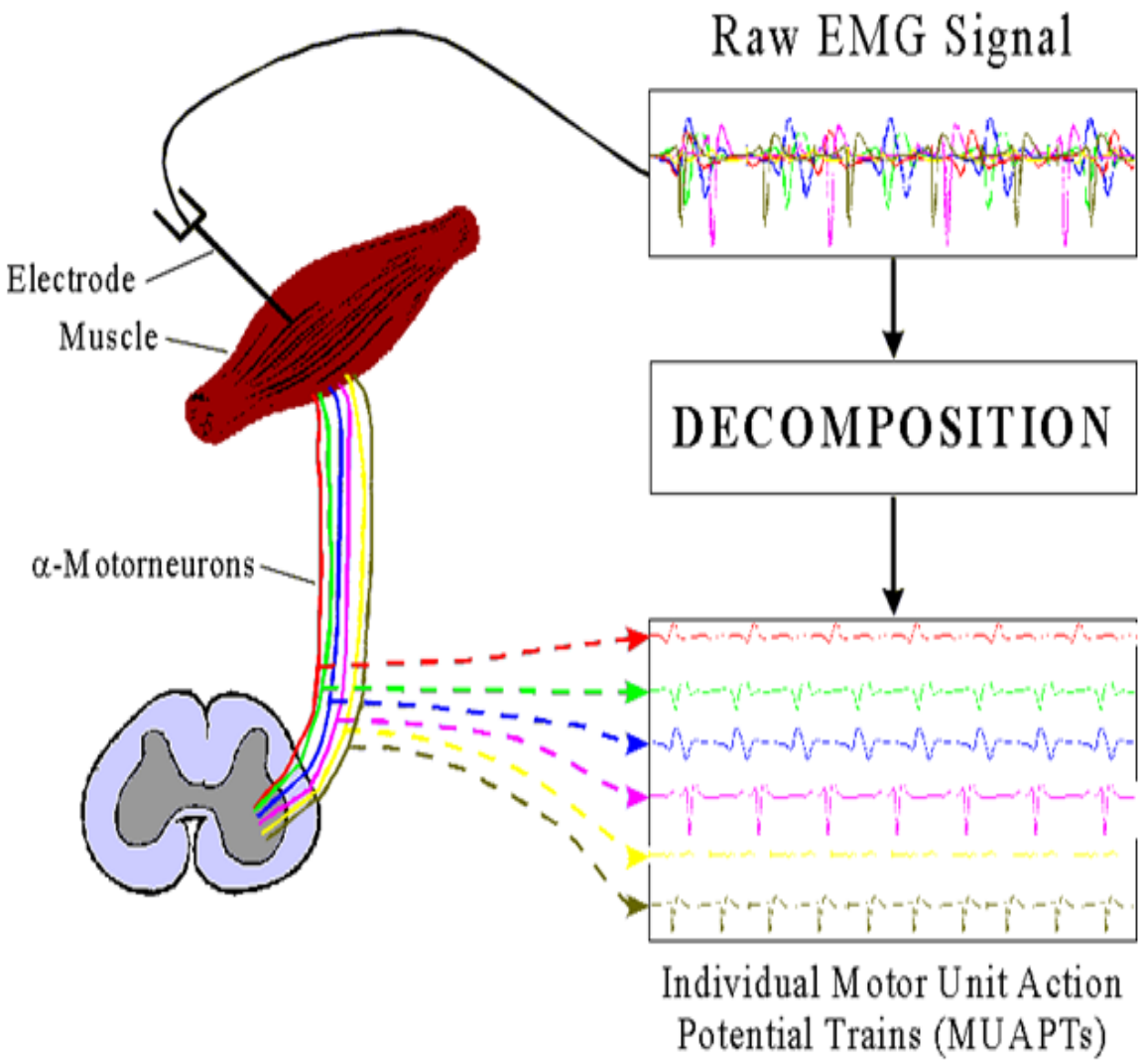

Figure 1 Pictorial outline of EMG signal decomposition used with permission from of the author[7]**.**

The alpha-motoneuron pool generates the firing patterns in the motor units of the muscle and these discharge patterns together combine to form the surface EMG. A raw EMG signal is a summation of several motor unit action potentials. To obtain the response of individual MUs, a decomposition algorithm is applied to the raw EMG signal. Thus, the contribution from each motor unit is derived from the raw EMG signal.

When the EMG signal contains the activity of large number of MUs the individual action potentials become impossible to differentiate because of the similarity among two or more MU action potentials [8]. After the decomposition is performed, the final step is to check the results. If there are gaps or uneven intervals in any of the discharge patterns, or if there are spikes in the signal that have not been accounted for (decomposition errors), then the decomposition is probably not correct. On the other hand, if all the activity in the signal has been adequately accounted for by a set of motor units with physiologically realistic discharge patterns, then there is a good chance that the decomposition is substantially complete and correct [9].

The decomposition of the raw EMG signal is used to study the motor control. To study the MU interaction different parameters are used such as common drive (CD), synchrony (CIS) in time domain and coherence in frequency domain.

1.6 Motivation for the study

This thesis deals with two separate issues, the first one is the CVD estimation technique proposed by Sundar.S, *et. al.* [3], where the experimental recording of the full CNAP from the elbow site was of concern. Three problems were detected: (1) consistency in stimulating the elbow site repeatedly over different trials, (2) the sampling frequency of 5 kHz was also a concern due to the frequency content of the antidromic full CNAP being recorded was found to have frequency components higher than 2.5 kHz, and (3) Some jitteriness is observed in some of the preliminary CVD estimates obtained for the wrist site due to a resolution issue due to short stimulating – recording distance. Also, the movement

artifact was usually recorded due to the presence of median nerve motor branches at the elbow site resulting in the recruitment of forearm muscles. Recording noise on the full CNAP seemed to have significant impact on CVD estimation

The second part of this thesis is about EMG decomposition errors. Decomposition algorithms misclassify MU firings which can lead to distortion in the parameters derived to study motor control. One of these parameters is the coherence function. Understanding the impact of these decomposition errors on the coherence function is the reason for this part of the study.

1.7 Objectives

In the first part, assessment of the protocol for CVD estimation using the collision technique led to possible changes in the experimental setup and the following objectives are set as part of the CVD estimation:

i. To consider a new stimulus location at the wrist for recording full CNAP to obtain CVD estimates. To compare the results of the CVD estimates obtained at elbow with wrist site in both simulations and experiments.
ii. To test the impact of two different sampling rates 5 kHz & 10 kHz. To apply a higher sampling rate of 10 kHz and compare the results obtained with 5 kHz sampling rate in simulations and experiments.
iii. Experimental recordings always contain a certain amount of noise. An assessment of the significance of signal to noise ratio (SNR) is performed by measuring the SNR level of the experimental recordings. This level of noise is incorporated to the

simulations in order to predict the estimator performance under experimental conditions. Smoothing techniques will be evaluated to overcome the resolution issue caused by shorter wrist – finger distance and also due to movement artifact when stimulated at the elbow.

The later part of this thesis discusses the EMG decomposition errors. Three types of errors are manually introduced to motor unit (MU) firings contained in 'error-free' decomposition files.

iv. The objective is to evaluate the impact of different levels of errors on the coherence function.

1.8 Thesis Outline

Chapter 2 presents an overview of the Collision Technique, recording of the CNAP, stimulating site currently being used to record the full CNAP, the effect of choosing appropriate sampling frequency, noise and its effects on signal recording is provided. Section 2.3 thru 2.6 provides an overview of the Electromyography, Signal decomposition & decomposition technique. Finally, the introduction to errors in EMG recording and coherence analysis to comprehend the effect of errors is introduced.

Chapter 3 describes the collision technique based CVD estimations and the improvements proposed to the existing method. Section 3.2 – 3.5 provide a brief introduction to stimulation site, sampling rate and smoothing techniques. The results of simulation study pertaining to the improvements has been presented and discussed in

section 3.6 through 3.7. In section 3.8 the results obtained from the experimental data are presented and discussed followed by section 3.9 with summary related to the simulation study and experimental results.

Chapter 4 discusses the impact of decomposition errors on EMG signal coherence. Various types of errors (FN, FP & FNP) and levels (1, 2,6,10 & 20 errors per 5 secs) are described in Section 4.1. Section 4.2 presents the method by which errors are introduced and coherence computation, it also shows the way the PMSE is calculated to obtain the performance measure of the coherence analysis. The results and discussion are presented in section 4.3 followed by section 4.4 with the summary of the chapter.

Finally, chapter 5 offers a summary of this thesis work and recommendations for future work.

CHAPTER 2 Literature Review

This chapter presents an overview of the conduction velocity distribution (CVD) estimation based collision technique used for this thesis and various methods to record the nerve response (CNAPs), stimulation site and sampling frequency. Attention has also been drawn on the noise affecting the CVD estimation. Electromyography (EMG) has been briefly discussed, in particular the process of decomposition of an EMG file. Finally, the effect of errors on the EMG recordings has been presented.

2.1 Collision Technique

Several researchers have conducted the studies dealing with nerve conduction velocity distributions [10, 11]. Non-invasive methods have been proposed for the estimation of CVD by various authors [12, 13]. As early as 1962 Hopf proposed conduction velocity distribution measurements based on the collision method [14]. In this method, a distal supramaximal stimulus is combined with a delayed proximal stimulus with the aim of CVD evaluation. When the inter stimulus interval (ISI) is relatively short, the proximally evoked orthodromic nerve action potential is cancelled by the antidromic impulse coming from the distal stimulus site as a result of the collision, only obtaining an early action potential at the recording site. By sequentially increasing the ISI, an instant is reached, at which the distally evoked antidromic impulse would have passed the proximal site before the proximal stimulus is delivered. Provided that the nerve fiber has recovered from the associated refractoriness, an orthodromic impulse would be initiated in response to the proximal stimulus, which, in turn, would evoke an additional late action potential

(test potential). When the whole nerve is considered, cumulative activation of fibers can be measured by recording the compound action potential (CAP), as the ISI is being gradually incremented. The fastest velocity corresponds to the ISI value at which the late action potential starts being observed in the recording, while the slowest velocity is found for the ISI at which this response reaches its maximum size.

i. Recording of the CNAP

The CNAP can be recorded through surface electrodes placed at the wrist or through ring electrodes placed at the digits. The amplitude of the responses is dependent on the distance between the nerve and the electrode [15]. Averaging over a few CNAPs is required to acquire an improved signal to noise ratio (SNR) [16]. The CNAP may be recorded using monopolar or bipolar electrodes. Bipolar electrodes have become more popular over time as the stimulus artifact is smaller. However the amplitude of the CNAP is influenced by the interelectrode distance due to phase cancellation. A distance of 3 – 4 cm between the surface electrodes is associated with the smallest distortion of latency and amplitude [17-19].

2.2 Stimulating Site

The key to a good diagnosis is stimulating and recording at the right sites. To record an evoked potential for diagnosis of CTS several stimulating and recording sites have been proposed. The most suitable sites to stimulate were determined to be the wrist and the elbow, the signal is recorded at the finger with the use of ring electrodes. Dawson described

the orthodromic measurement of sensory nerve conduction velocity (NCV) as the impulses generated by stimulation travel in the direction in which sensory nerves normally conduct, from the periphery toward the center and in this type of measurement the stimulation site is typically at the finger and the response is acquired at the wrist [20]. Sears was the first to record a diphasic potential from the fingers evoked by stimulation at the wrist. It was identified as an antidromic sensory conduction because the nerve fibers examined conducted in a direction opposite from the normal [21].

Buchthal and Rosenfalck compared the antidromic with orthodromic sensory potentials. The antidromic response is larger than the orthodromic response recorded using surface electrodes because the digital nerves are nearer to the surface than the nerves at the wrist. A study conducted shows that the antidromic method produced nerve action potentials of greater amplitude. The distance between the recording electrode and the nerve is an important variable because with the increase in distance the amplitude of the CNAP reduces progressively [22-24].

Because of different rates of conduction of different-sized myelinated fibers, the CNAP becomes more dispersed as the distance between the recording and the stimulating electrodes is increased. When the position of the recording electrode was changed from the wrist to the elbow the sensory CNAPs recorded with the needle electrodes showed a drop of 75% in amplitude in the orthodromic median nerve conduction [22]. The drop in amplitude was found to be approximately 50% when the stimulating electrode was shifted from the wrist to the elbow in the antidromic conduction [24]. With bipolar placement the surface electrodes, have been used to record the potentials [19].

2.3 Sampling Frequency

Most biological electrical potentials consist of a combination of complex discharges with variable frequencies. Fourier analysis of these complex discharges reveals the sum of sine waves of different frequencies as their constituents. In general neurological tissue has frequencies ranging from 5 to 10 kHz. Activities outside this range are most likely to be artificial and hence should not be included in analyses [25]. For this reason an appropriate sampling frequency is essential to retrieve the required signal data. The Nyquist theorem states that if a signal contains frequency components ranging from 0 to f_s, then the minimum sampling frequency that can be used to adequately represent the frequency content of the original signal is $2f_s$, the Nyquist frequency. This sampling frequency is the minimum necessary to avoid aliasing distortion of the input signal.

In the antidromic NCV measurement it is difficult in determining precisely the start of the nerve action potential, especially in those cases with small amplitudes. This is of particular importance when conduction velocities are measured along short distances. The error of latency measurement in orthodromic nerve conduction studies is negligible. However, a larger sampling frequency may be necessary in some cases to achieve adequate resolution of finer details in the recordings [26].

2.4 Signal to noise ratio

Experimental measurements are never perfect, even with sophisticated modern instruments. Two main types or measurement errors are recognized: systematic error, in

which every measurement is either less than or greater than the "true" value by a fixed percentage or amount, and random error, in which there are unpredictable variations in the measured signal from moment to moment or from measurement to measurement. This latter type of error is often called noise. There are many sources of noise in physical measurements, such as building vibrations, air currents, electric power fluctuations, stray radiation and from nearby electrical apparatus.

The quality of a signal is often expressed quantitatively as the SNR which is the ratio of the true signal amplitude (e.g. the average amplitude or the peak height) to the standard deviation of the noise. Measuring the signal-to-noise ratio usually requires that the noise be measured separately, in the absence of signal. However, if the magnitude of the noise depends on the level of the signal, then the experimenter must try to produce a constant signal level to allow measurement of the noise on the signal. The relative amplitude and the background noise must be taken into consideration to avoid falsely interpreting the noise as the neural response. Sometimes the two can be partly distinguished on the basis of frequency components: for example, the signal may contain mostly low-frequency components and the noise may be located at higher frequencies. This is the basis of filtering however something that distinguishes signal from noise is that random noise is not the same from one measurement of the signal to the next, whereas the genuine signal is at least partially reproducible. A simple and widely used method for removing the background noise is by averaging many epochs of the signal. By averaging several recordings with the same repeating stimuli, the activities unrelated to the stimuli will cancel out and only true evoked responses remain visible because they are time locked to the onset of the stimulation. This is called ensemble averaging, and it is one

of the most powerful and commonly used methods for enhancing signal quality when it can be applied. In general the SNR improves in proportion to the square root of the number of epochs averaged. For example, averaging four responses improves the SNR by a factor of two [16].

ii. Noise of Surface electrodes

Recordings of biomedical signals from the body surface often contain a substantial noise component. This noise signal can severely impair the resolution of biomedical recordings [27]. The electrodes are for the major part responsible for the noise in interface and can contribute to the noise of surface electrodes surface biopotential recordings.

Gondran investigated the noise from electrodes placed on the skin and found that the recorded noise decreases with increasing frequency [28]. For low frequencies, the noise is much higher than the equivalent thermal noise generated in the impedance of the electrodes and skin.

During the recording of biomedical signals, despite relaxation, muscles always show a basic level of electrical activity. It has been suggested that this residual EMG activity may constitute a significant part of the total noise level [27, 29, 30]. Godin also indicated that the noise of the amplifier can be of importance. When a surface electrode is applied to the skin, the skin is included in the functioning of the electrode. Geddes reported that the noise of electrodes depends on test subject, electrode gel and skin preparation [31].

A decrease in noise of up to 50% is reported in the first 20 min after application of

wet-gel electrodes. The wet- gel electrodes can advantageously be applied to the skin some time before the recordings are made. The noise of electrodes has been reported to be inversely proportional to the square root of the area of the electrode on the skin. If the desired spatial resolution permits, large-area electrodes should be preferred in low-noise recordings [32]. Further discussion about the stimulation site, noise and to determine the appropriate sampling frequency is available in chapter 3.

2.5 Eletromyography

EMG is a technique for evaluating and recording the muscle responses. An electromyogram is recorded with the help of needle or surface electrodes. The electrodes detect the electrical potential generated by muscle cells that are activated electrically or neurologically. The signals can be analyzed in order to detect medical abnormalities or analyze the biomechanics of human movement.

2.6 Signal Decomposition

EMG signals are essentially made up of superimposed MUAPs from several motor units. The decomposition of the EMG signal is the procedure by which the signal can be decomposed into their constituent motor unit action potential trains (MUAPTs). In the clinical environment, measurements of some characteristics of the MUAP wave form (shape, amplitude and time duration) are used to assess the severity of the neuromuscular disease or in some cases to assist in making the diagnosis. Signal decomposition is a technique where motor unit action potential trains are extracted from the EMG signal using

a computer assisted interactive algorithm. The algorithm uses continuously updated template matching routines and firing statistics to identify the MUAPs in the EMG signal. The templates of the MUAPs are continuously updated to enable the algorithm to function even when the shape of a specific MUAP undergoes slow variations [7].

iii. Decomposition Technique

In the clinical environment, measurements of some characteristics of the MUAP waveforms such as shape, amplitude and time duration are considered to assess or diagnose the severity of a neuromuscular disease. Thus the decomposition of the signal is essential. The myoelectric (ME) signals are decomposed into their constituent MUAPT's (see figure 1) by the Precision Decomposition technique to obtain the map of MU firings. The output of the EMG decomposition algorithm is a set of impulse trains. Each impulse corresponds to a firing of the appropriate motor unit [8].

1. The manual decomposition was used before the introduction of computers, in such method EMG signals were recorded photographically from the oscilloscope screen and then decomposed manually by marking the repetitive occurrences of each distinct spike. With the advancement in technology, computers are used, however the process is largely the same and it involves three major steps. Different MUAPs are determined by categorizing the spikes in the signal on the basis of their shapes. The spikes that have similar shapes are possibly from the same motor units, while spikes with unique shapes are likely to be superposition of two spikes.

2. Once the spikes are differentiated based on their shapes, the next step is to classify or assign them to the MU from which they originated. The motor-unit discharge patterns can be used to help determine which motor units are involved. In this way it is usually possible to work out the number of different MUAPs and to establish templates of their shapes.
3. The final step in decomposition is to verify the results based on the inter-spike interval (ISI). The decomposition is considered complete if all the activity in the signal has been adequately accounted for by a set of motor units with physiologically realistic discharge patterns. And if there are gaps or uneven intervals in any of the discharge patterns, then there is a possibility that the decomposition is incomplete.

It is possible that some signals and some MUAPTs within the signals can be decomposed more reliably than others. Decomposability depends on several factors including the complexity of the signal, the level of background noise, the variability of the MUAP waveform from the same motor units, and the similarity of the MUAPs from different motor units [33].

2.7 Firing rate estimation

The firing activity of a MU is represented by the times at which the actual firing occurs and the firing rate information is derived from these firing times. The firing time information for a MU active during a contraction is derived with the help of decomposition algorithms that require needle EMG signals to provide information regarding the firings of

each MU that is identifiable [10]. The inter-firing interval (IFI) over a certain number of firings is averaged to obtain the mean firing rate estimate based on the firing times [35].

2.8 Decomposition Errors

Decomposition errors arise primarily because often a motor unit train seems to split into two or more trains due to shape differences among MUAPs of the original train. Decomposition algorithms may also fail to identify MUAPs of different MUs when they fire concurrently causing superposition of several of these potentials. The errors are classified into three types; False Negative (FN), False Positive (FP) and False Negative Positive (FNP). When the MU firing is not recognized by the algorithm it is known as a FN type of error, additional firings not belonging to the MU are added in the FP case. And the FNP type of error is a miss- assignment which is the case of one MU firing being assigned to another MU [33].

2.9 Coherence Analysis

Coherence gives information on the degree of dependency between two signals recorded in the frequency domain. Analysis of coherence between simultaneously active motor units has revealed several distinct drives to the motoneuron pool during isometric contraction. These include coherent activity at 1–2 Hz which may also be detected as the common modulation of mean motor unit firing rates termed ‘common drive’ [36].

The coherence computation is implemented as mscohere in Matlab. The squared magnitude coherence provides a bounded measure of linear association between the two

series, taking on a value of 1 for perfect linear relationship and a value of 0 if the series are uncorrelated. *Cxy* (*f*) varies between zero and one and is defined as,

$$C_{xy}(f) = \frac{|S_{xy}(f)|^2}{|S_{xx}(f)S_{yy}(f)} \qquad \textbf{Eq. 2}$$

Where *Sxx*(*f*) and *Syy*(*f*) are the autospectral density functions of *x*(*t*) and *y*(*t*), and *Sxy*(*f*) is the cross-spectral density function between *x*(*t*) and *y*(*t*) [37].

The decomposition algorithm is prone to errors even with sophisticated algorithms. To assess the impact of errors on the EMG signal, coherence is used as a parameter to establish the error tolerance of the decomposition algorithm. Further discussion on coherence analysis and its use in this thesis is provided in chapter 4.

CHAPTER 3 Collision CVD Estimation – Experimental Protocol

This chapter discusses three parameters that can help improve the CVD estimation; the stimulation site for the full CNAP (elbow vs. wrist), sampling rate and finally the smoothing techniques. The collision technique based CVD estimation to determine the severity of the carpal tunnel syndrome is used to make the improvements mentioned. A method to estimate the CVD using the collision technique was described by Sundar, S. et al [3]. In this method the source was estimated from the CNAP difference, which was found by subtracting two CNAPs recorded at the middle finger upon stimulating the median nerve at both the elbow and the wrist sites with different ISIs for each collision. The CNAP difference contains the contribution from nerve fibers within the velocity interval determined by the two ISIs. Then the CVD is estimated using the electrical source and a full CNAP recorded at the finger upon supramaximal elbow stimulation.

Preliminary results obtained using the CVD estimation protocol suggested by Sundar.S showed that the full CNAPs obtained from the elbow site were inconsistent. To overcome this problem, a change in the experimental protocol has been suggested and implemented to find a more suitable location to obtain the full CNAP with a higher likelihood of recruiting the same set of fibers repeatedly. In the modified protocol, the objective was to investigate if by obtaining the full CNAP from wrist stimulation CVD estimates were more consistent. This approach has the advantage that it is relatively easier to stimulate at the wrist location.

Figure 2 shows the change in the protocol, stimulation at wrist site (S2) for the full CNAP to obtain the CVD estimate. On the other hand, different distances; *i.e.* elbow-finger vs. wrist-finger, produce different delay dispersion, which in turn may affect the CVD estimation especially when the stimulation-recording distance is short. Hence, CVD results obtained from elbow CNAPs were compared to those obtained from wrist CNAPs. Based on the analysis of the raw CVD estimates obtained from the wrist, CNAP smoothing techniques were applied in order to seek an improvement of the CVD estimates. The results before and after the smoothing and filtering were compared using the percent mean square error (PMSE) as performance index. Different sampling frequencies were tested in simulations and experimental work to determine the appropriate sampling frequency used to collect data.

3.1 Collision Technique

The collision technique in nerve conduction studies (NCS) uses a nerve response obtained by applying two stimuli at two different sites along the same nerve this is the collision of proximal and distal impulses. Two stimulation channels are placed on the skin surface, one at the wrist (the distal) and another at the elbow (the proximal). The proximal and distal CNAPs are recorded using a bipolar channel consisting of two surface ring electrodes placed at the middle finger. When the ISI is gradually decreased, the contribution from small nerve fibers reduces as the slow traveling action potentials generated at both stimulation sites start colliding and only the faster traveling action potentials are recorded by the ring electrodes placed on the finger.

The CVD estimation based on the collision technique proposed by Sundar, S. et al [3]

has been evaluated for changes in the following parameters: stimulation site, sampling frequency, recording noise and finally the smoothing techniques. The experiments are performed with the approval of the “Health Sciences Human Research Ethics Board, Dalhousie University” (see Appendix B).

3.2 Stimulating Site

By stimulating at the elbow for the full CNAP, it was found that the stimulating location is not consistent. The placement of electrodes is considerably difficult in muscular subjects and the median nerve being located deeper compared to the wrist site. With the placement of the electrodes being inconsistent the inaccuracy in obtaining the same set of fibers for consecutive recordings is high.

Another issue when stimulating at the elbow is that motor branches of the median nerve are recruited, causing movement of the hand where the recording electrodes are placed. The movement artifact is quite influential on the CNAP recording resulting in unwanted information or noise. Due to these inconsistencies, it was decided to try another location and obtain the full CNAP from the wrist. The wrist has been chosen for obtaining the full CNAP as the stimulating electrodes can be placed at this site with almost no error for different recording sessions and different subjects. No motor branches are activated upon stimulation at the wrist and the median nerve is located closer to the skin surface, making it a suitable place as a stronger full CNAP can be recorded with lower stimulus intensity. A pictorial representation of the change in the protocol and the electrodes placement is shown in Figure 2.

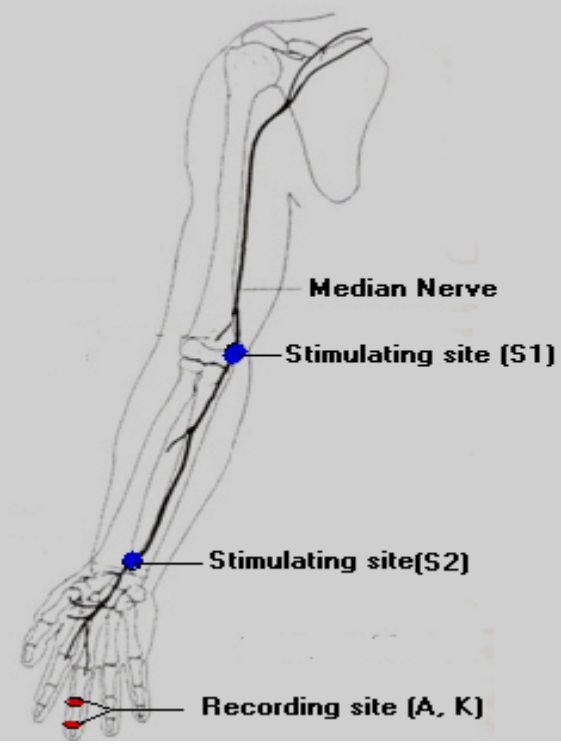

Figure 2 Electrode placement showing the change in the protocol

Figure 2 shows the electrode placement for stimulation of full CNAP. The S1 and S2 are the elbow and wrist stimulation sites. The full CNAP is recorded at the finger A & K (A – anode and K – cathode). The experimental methods and data analysis is discussed in later part of this chapter.

3.3 Sampling Rate

Particular attention was directed to the sampling frequency after changing the stimulating site from elbow to wrist. The sampling frequency being used earlier was 5 kHz in the protocol proposed by Sundar. S. It was suspected that there was signal present above 2.5 kHz frequency in the source and full CNAP whose dismissal may contribute to inaccuracies in the CVD estimation.

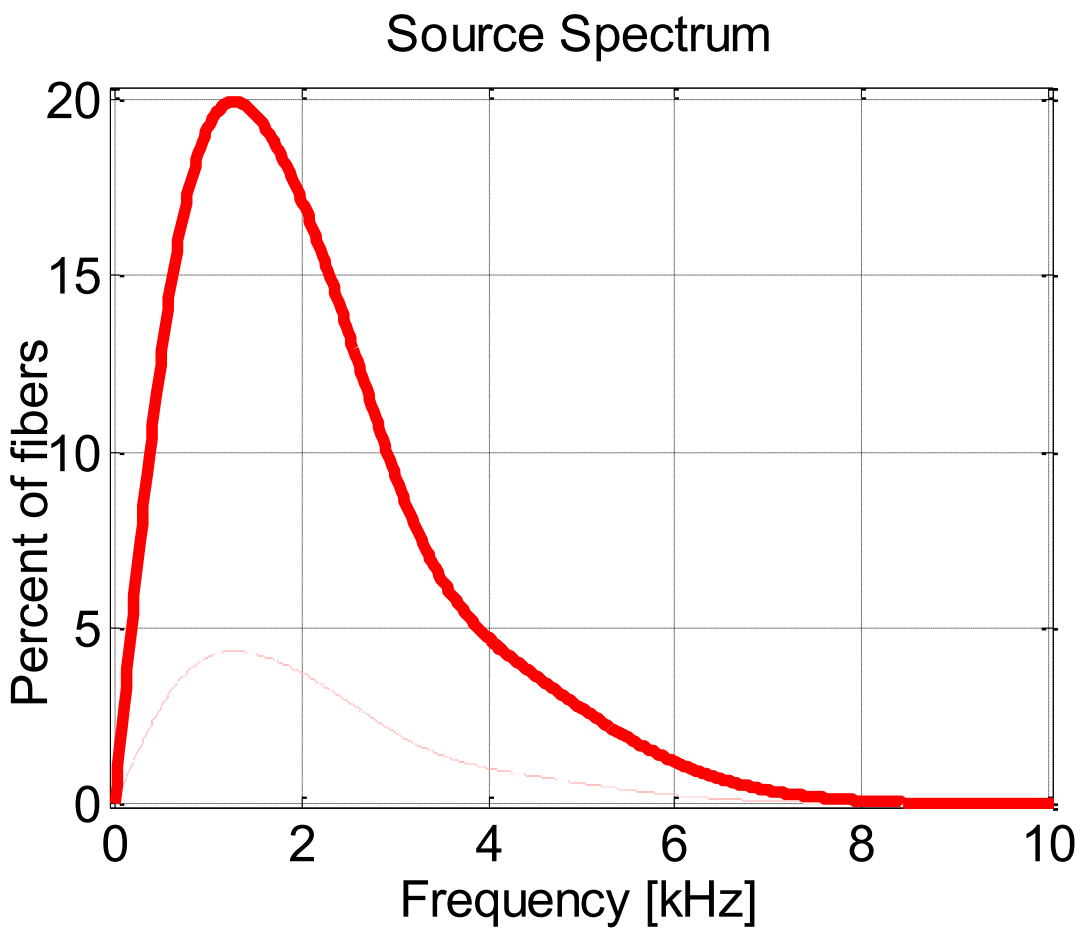

Figure 3 Simulated spectrum of the source.

Figure 3 show the spectrum of the electrical source, the first derivative of the transmembrane potential and the spectrum of a full CNAP recorded at the finger, it was realized that about 50% of the signal information exceeds 2.5 kHz frequency.

Thus, it was decided to investigate the effect sampling frequency has on the CVD estimation by increasing the sampling frequency to 20 kHz in the simulation study. To further understand the impact that sampling frequency has on the CVD estimation simulations were performed. CNAPs were simulated and sampling rates of 5 kHz and 20 kHz were used. The results of the CVD estimation were compared based on the site of

stimulation, sampling frequency and the smoothing techniques. To verify the simulation results the experiments were performed and sampling rates of 5 kHz and 10 kHz were used.

To better understand and verify if the full CNAP had a contribution above 5 kHz sampling rate. The simulated spectrum of the full CNAP was plotted (see Figure 4). It was found that about 40% of the fibers exceed over 2.5 kHz frequency range. To understand how much these components stretching beyond 2.5 kHz can assist in estimating a better CVD the sampling rate was increased from 5 kHz to 20 kHz in simulations. The results obtained with both sampling rates were then compared to assess improvement.

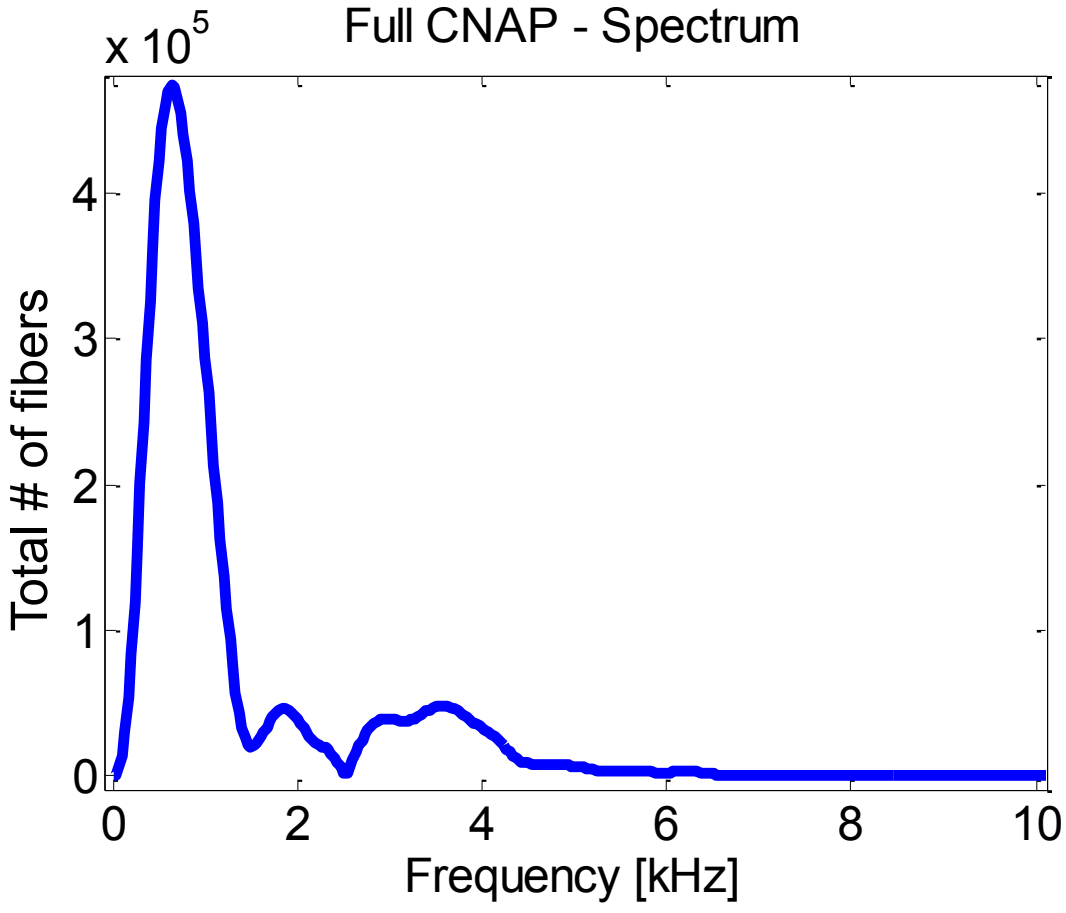

Figure 4 Simulated spectrum of a full CNAP elicited from wrist stimulation.

3.4 Recording Noise

To acquire readings of the noise alone, a segment of the baseline before and after the occurrence of the signal was taken. To perform the simulations, noise level in the signal is computed by obtaining the standard deviation of the noise in the experimental recording and applying the same level of noise in the simulations to replicate the experimental conditions. Gaussian noise was added to each of the three signals; Full CNAP, CNAP ISI 1 and CNAP ISI 2.

The SNR was found as,

$$SNR = A / \sigma \qquad \textbf{Eq. 1.}$$

Where A is the maximum value of the CNAP and σ is the standard deviation of the noise. The SNR value estimated from experimental recordings was found to be approximately 16 for a full CNAP. This SNR level was later introduced to the three signals (full CNAP, CNAP_ISI1 and CNAP_ISI2) in simulations as mentioned earlier.

3.5 Smoothing Techniques

After observing the experimental recording and studying the effect of noise on the signal in simulations a further study revealed that a method was required to lessen the impact of the recording noise on the CVD estimate. Two techniques were determined suitable for a close approximation of the CVD estimate to the actual CVD. These techniques were smoothing techniques. The smoothing techniques help better estimate the

CVD and achieve greater precision and a closer match to the actual CVD.

3.6 Smoothing of CVD Estimate

Smoothing of the CVD was performed to improve the CVD estimate and get close to the original CVD response. The smoothing technique was used to reconstruct the distorted CVD estimate sampled at 5 kHz and was later extended to the CVD estimates at 20 kHz sampling rate (see Figure 5). The smoothing function smoothes the data, using a running mean over 2*N+1 successive points, with N=3 points on each side of the current point. At the ends of the series skewed or one-sided means are used.

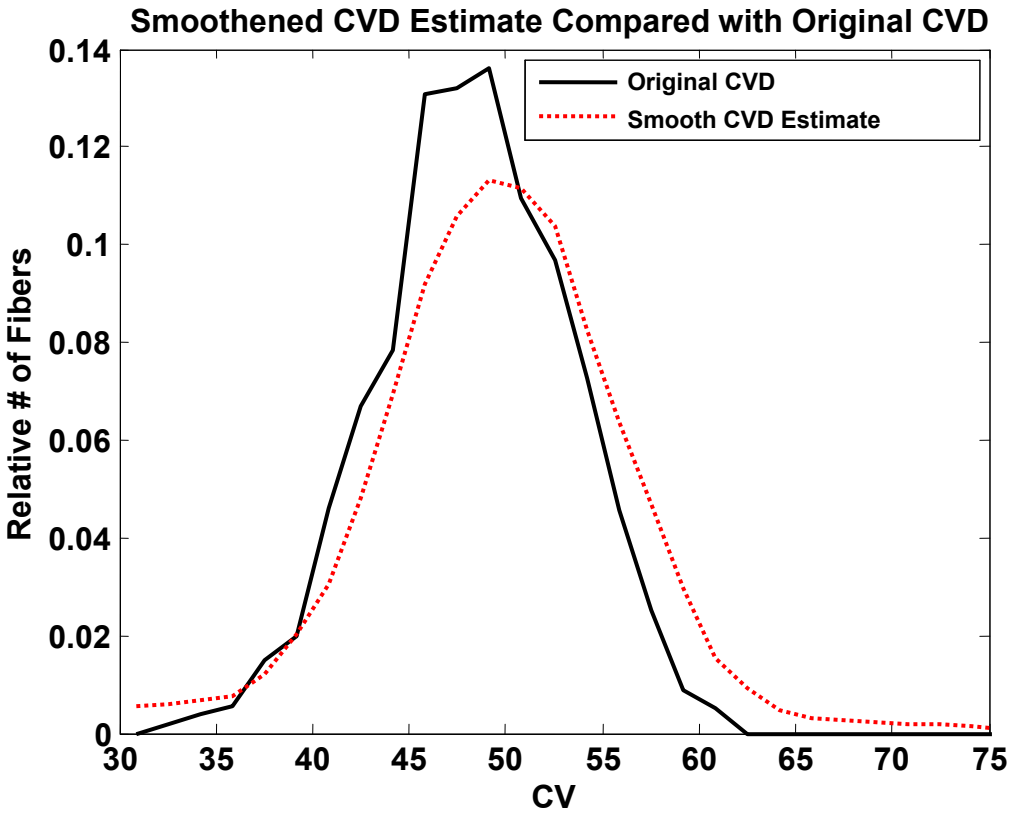

Figure 5 Simulated Smoothed CVD estimate compared with original or actual CVD.

To establish a standard for comparison in simulations a template CVD was generated with no jitteriness, this CVD is referred to as original/actual CVD in simulations. Looking at Figure 5 it can be said that the smoothed CVD estimate (dotted red line) follows the actual CVD (black solid line) very closely. Further discussion on the simulations results are discussed in the following sections of this chapter.

3.7 Filtering of CVD Estimate

The second technique used to smooth the CVD estimate was obtained through low-pass filtering. A low pass filter was designed to pass low-frequency signals and limiting the higher frequency signals that make the CVD estimate jittery, thus obtaining a close approximation of the CVD estimate to the inital CVD. A 5^{th} order low pass filter was designed using the window method in MATLAB with the fir1 function. This is a Hamming-window based linear-phase filter with normalized cutoff frequency ωn, which is a number between 0 and 1, where 1 corresponds to the Nyquist frequency. A value of ωn = 0.2 was found to offer the best results. In the sensory nerve conduction, the high frequency is important because of the shorter duration of the potentials. The reduction of the high frequency limit decreases the amplitude and increases the latency.

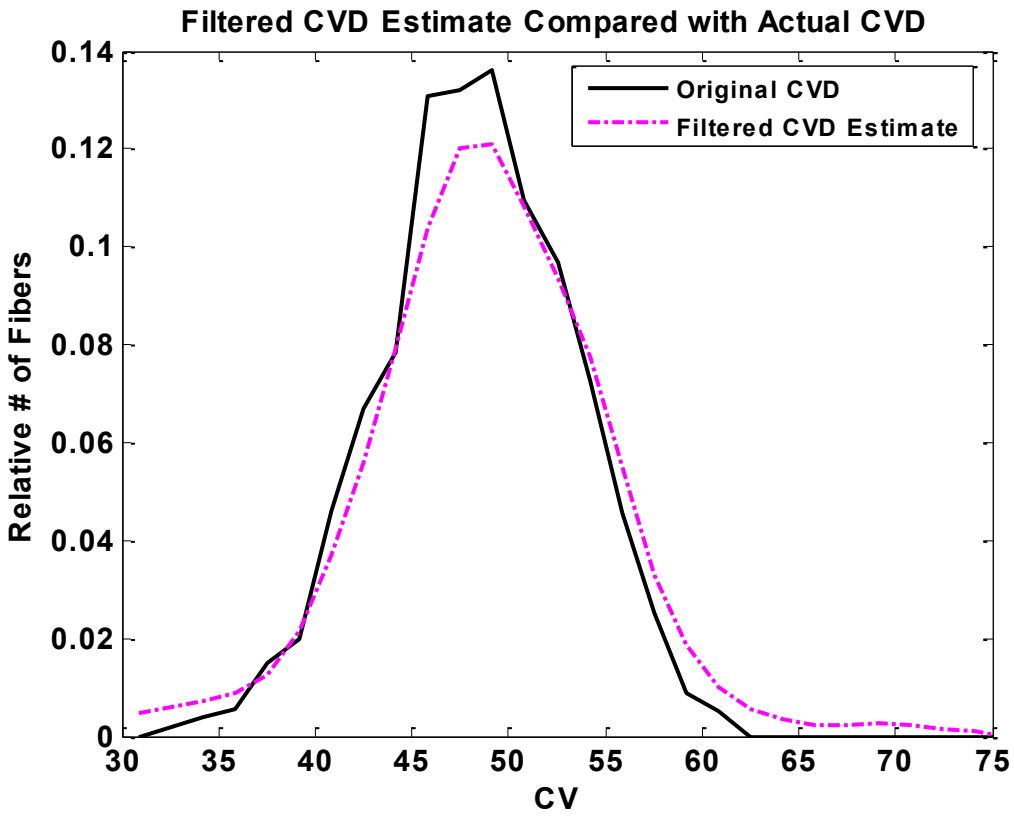

Figure 6 Filtered CVD estimate compared with the original or actual CVD.

Figure 6 demonstrates the improvement in CVD estimate can be achieved by filtering (magenta dashed line) and a closer approximation to the actual CVD (black solid line) can be seen. In order to compare the initial CVD estimate, the smoothed CVD estimate and filtered CVD estimate Percent mean square error (PMSE) was used as a performance index.

The error between the true CVD estimate and the estimates obtained was found using the PMSE,

$$\mathbf{PMSE} = \frac{\boldsymbol{mean}\{(\boldsymbol{w}-\boldsymbol{v\_pdf})^2\}}{\mathbf{max}\{(\boldsymbol{v\_pdf})^2\}}\mathbf{x100} \qquad \textbf{Eq. 2.}$$

where w is the CVD estimate, and v_pdf is the actual velocity pdf used for generating the CNAPs in simulations.

3.8 Simulations

Simulations were performed in MATLAB to determine the affect of individual parameters. A detailed comparison has been done between the initial CVD estimate, smoothed CVD estimate and the filtered CVD estimate. The performance of all the three estimates was evaluated for various parameters, such as stimulation site, sampling frequency and recording noise. The results presented as part of the simulations are an average of 10 trials.

3.8.1 Simulations Results

The initial idea about trying the sampling rates and the stimulation sites was tested using simulations. The simulation study was conducted using two sampling frequencies 5 kHz and 20 kHz. The sampling frequencies were tested on the different stimulation sites, Wrist and Elbow. When stimulating at the elbow site the recruitment of the same set of nerve fibers is difficult each time an experiment is performed. The other reason is the recruitment of flexor muscle causing a great deal of movement in the hand as different subjects have varied sensitivity to the stimulation. When the wrist is stimulated the recruitment of nerve fibers is considered to be relatively easy every time the experiment is conducted and the CNAP response is much greater than at elbow site even for lower stimulus intensity.

Figure 7 shows the combined plot of CVD estimates for 5 kHz (dotted green line)

and 20 kHz (dotted blue line) along with actual CVD (solid black line) obtained using a full CNAP elicited at the wrist. It can be noticed from the figure that the CVD estimate with 5 kHz is jittery and has poor CVD estimate compared to that of the initial CVD estimate, but at 20 kHz the CVD estimate is a closer match to the actual CVD.

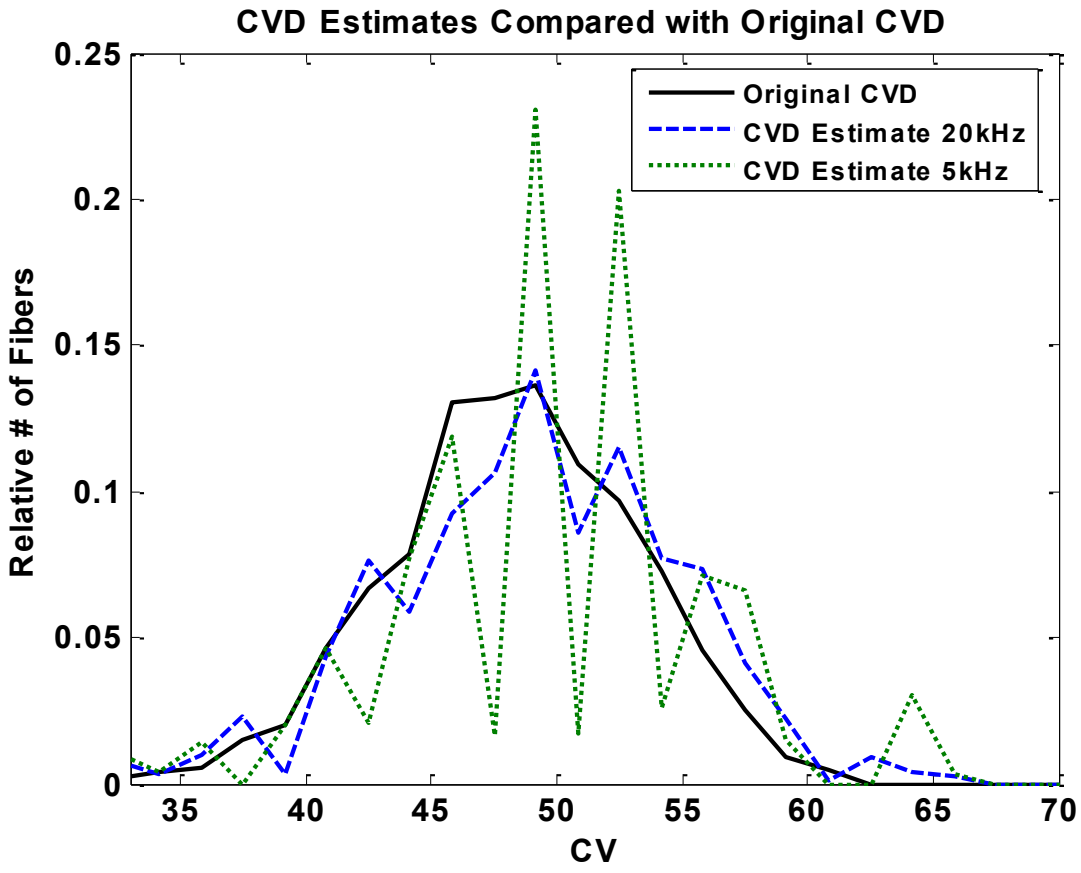

Figure 7 Comparison of CVD estimates using a full CNAP elicited at the wrist.

Figure 8 shows the CVD estimates for 5 kHz and 20 kHz along with actual CVD obtained using a full CNAP elicited at the elbow. The CVD estimate obtained whit the full CNAP from the elbow has less jitteriness for the CVD estimate with 5 kHz. And at 20 kHz the CVD estimate is a much close to the actual CVD.

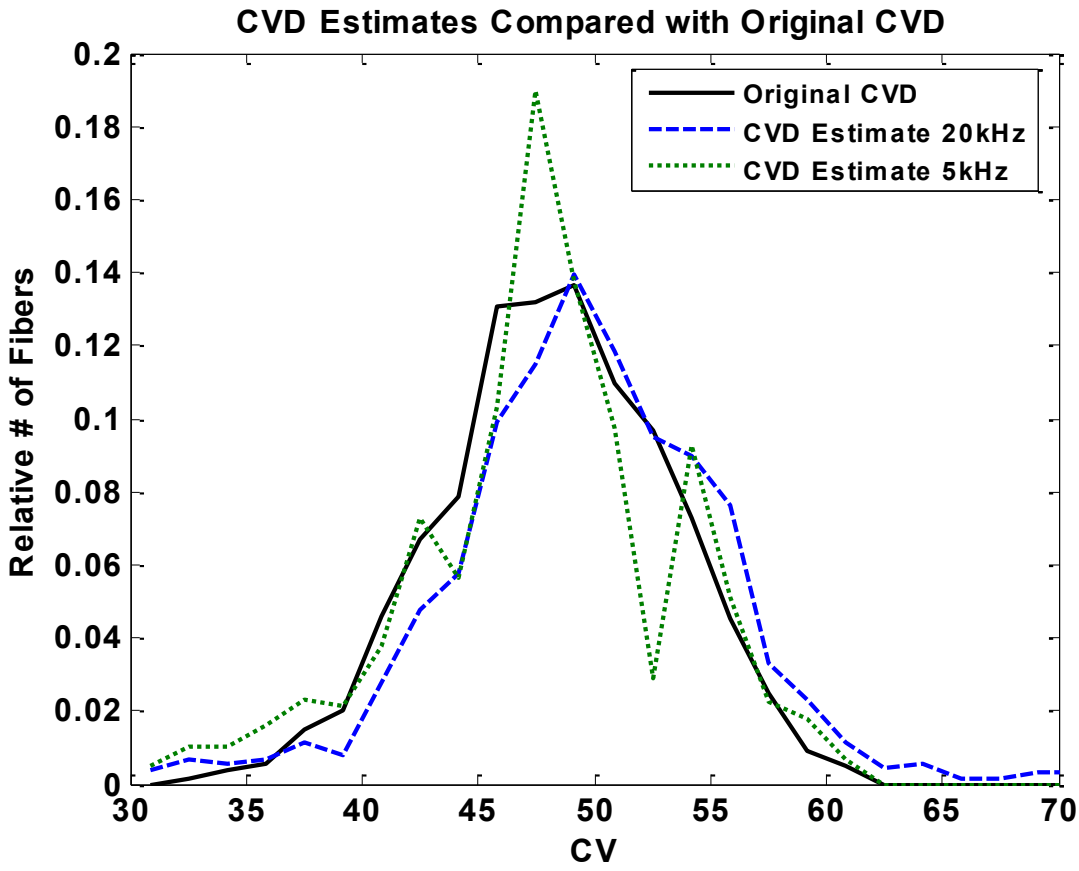

Figure 8 CVD estimates comparison at a sampling rate of 5 kHz and 20 kHz using a full CNAP elicited at the elbow.

A comparison of the CVD estimates with different sampling rates has been presented in Table 3-1 which is obtained by finding a percent error between the actual CVD and the CVD estimates for 5 kHz and 20 kHz.

Table 1 Comparison between different stimulating sites (elbow & wrist).

Site of stimulation	PMSE - 5 kHz	PMSE - 20 kHz
Elbow	1.8504	0.7730
Wrist	9.0236	0.9451

Table 1 presents the results obtained for the CVD estimates shown in figures 7 & 8. It can be seen that with the increase in sampling frequency from 5 kHz to 20 kHz, CVD estimates from both wrist and elbow sites yield comparable results with lower error rates as observed in the third column.

To understand how the noise effects the CVD estimates with no noise and CVD estimate with noise equivalent to that of the experimental noise, SNR equal to 16 have been compared. These conditions were tested in the simulations for 5 kHz and 20 kHz. Tables 3-2 – 3-4 show results obtained for CVD estimates with no noise and noise equivalent to experimental noise (SNR = 16) for different sampling rates.

Table 2 Average PMSE values for 5 kHz & 20 kHz with and without noise.

Estimate	**No noise**		**With noise (SNR =16)**	
	Fs = 5kHz	**Fs = 20kHz**	**Fs = 5kHz**	**Fs = 20kHz**
CVD estimate - Elbow	2.2099	0.6295	2.1421	0.6455
CVD estimate - Wrist	7.9032	1.0007	8.6687	3.0243

From the results presented in Table 2 it can be said that PMSE values at sampling rate of 5 kHz have small difference however with the increase in sampling rate to 20 kHz and addition of noise the results obtained from the elbow site are much better than that of the wrist, whose error improves with respect to 5 kHz but is greater than that of the error at elbow site.

A detailed comparison has been done between the initial CVD estimate and the CVD estimates obtained after implementing the smoothing techniques. The performance of all the three estimates was evaluated for various parameters; stimulation site, sampling frequency and recording noise (Tables 3 & 4). Under the experimental conditions there is always certain amount of noise in signals however to understand the effect of noise an ideal condition of no noise was simulated and a review has been presented. Values shown correspond to the PMSE calculated with respect to the actual CVD.

Table 3 Comparison between wrist and elbow sites for different sampling rates with no noise

Estimate	Wrist	Elbow	Wrist	Elbow
	Fs = 5 kHz	Fs = 5 kHz	Fs = 20 kHz	Fs = 20 kHz
Inital CVD estimate	7.9032	2.1421	1.007	0.6295
Smoothed CVD estimate	0.8975	0.6104	0.9519	0.7423
Filtered CVD estimate	0.4546	0.5601	0.4357	0.2606

It can be seen from the Table 3 that the initial CVD estimate error for the wrist site is 4 times higher at a sampling rate of 5 kHz compared to elbow site. When the sampling rate is increased from 5 to 20 kHz the error decreases significantly from 8% to 1%. Though when compared to the elbow site the wrist site still has approximately 40% higher error rate. However after applying the filtering the CVD estimate improves considerably and at a lower sampling rate of 5 kHz the error at wrist is 0.11% smaller. At a higher error rate of 20 kHz wrist error rate is twice that of the elbow site.

Table 4 Comparison between wrist and elbow stimulation sites for different sampling rates with noise

Noisy Condition	Wrist	Elbow	Wrist	Elbow
Estimate (PMSE)	**Fs = 5 kHz**	**Fs = 5 kHz**	**Fs = 20 kHz**	**Fs = 20 kHz**
Inital CVD estimate	8.6687	2.2099	3.0243	0.6455
Smoothened CVD estimate	1.4827	0.5476	1.2735	0.7944
Filtered CVD estimate	1.0761	0.4997	0.9047	0.3142

Table 4 shows the simulation results after the noise equivalent to that of the experimental level is introduced. For the wrist case, at 5 kHz the error is close to 9% it reduces by three times to 3% at 20 kHz. The error for elbow site reduces by almost 4 times with an increase in the sampling rate from 5 kHz to 20 kHz. The overall error at elbow site is lower than that at the wrist however the error rate decreased significantly in the wrist case after the filtering is employed; up to 7% at 5 kHz and by three times for 20 kHz sampling rate. The error increased after employing the smoothing function for the elbow site at 20 kHz this is caused due to the skewness of the CVD estimate resulting in increasing error than that of the initial CVD estimate.

With an increase in sampling rate from 5 kHz to 20 kHz, stimulation at the elbow site achieves better estimate even before the application of smoothing techniques. This can be due to the distance from stimulation to recording site which causes the delay dispersion to be more significant when stimulating at the elbow than at the wrist.

3.9 Discussion

For the results obtained with a sampling frequency of 5 KHz it can be seen that there are certain spikes and the estimate has an irregular shape. While the results obtained for the higher sampling frequencies of 20 kHz have relatively lower error with less jitteriness. After performing the filtering it was found that the estimates improved considerably. This can be seen from the Tables 3 & 4 that shows the PMSE readings tabulated for the sampling frequency of 5 and 20 kHz. At a sampling rate of 5 kHz after applying the filtering the error at the wrist site reduces by 8 times, whereas the error at the elbow site reduces by approximately 5 times. At a higher sampling rate of 20 kHz the error at wrist site decreases by almost 3 times and for the elbow site the error goes down by 2 times.

It can be observed from the tables that the initial CVD estimate for the high frequency of 20 kHz is better than the estimate obtained for 5 kHz. The smoothing and filtering processes improve the estimates for 5 kHz matching it to those with higher frequency. After smoothing techniques are introduced the estimates amplitude decreased, while the estimate spreads over a certain velocity range and acquires a smooth or steady rise and fall in the sides/edges.

Figures A1 through A4 in the appendix illustrate the difference between the actual CVD, initial CVD estimate and the CVD estimates obtained after smoothing and filtering. The resolution of the CVD estimate can be improved by employing the smoothing techniques and in particular the filtering. This improvement can be seen from the Table 4.

The initial CVD estimate in Figure A1, the blue dashed line is more jittery than the

actual CVD, the black solid line. Figure A2 shows that a better CVD estimate can be achieved with the increase in the sampling frequency. The increasing in sampling frequency from 5 kHz to 20 kHz improves the inital CVD estimate also leading to much smoother CVD estimates after applying the smoothing techniques. When the full CNAP is collected from the wrist to estimate the CVD the PMSE is higher than that at the elbow site. However by applying the smoothing techniques the error can be reduced.

Table 4 shows how much impact the increase in sampling frequency has on the CVD estimation. It can also be seen that the filtering outperforms the smoothing process producing an estimate closer to the actual CVD. Another interesting point to note is that by using the elbow as the stimulation site for the full CNAP the results obtained have lower error and smoother (see Figures A3–A4). It is believed that this is due to the distance between the stimulation site (elbow) and the recording site (finger) which is longer than that of the wrist – finger increasing the delay dispersion.

3.10 Experimental Methods, Analysis and Results

To test the change in the protocol the data was collected from 2 subjects; male, age range between 25 and 40 years both the subjects had healthy median nerves, no signs of CTS. Due to thoroughly distorted or very noisy CNAP detections some recordings are dropped from the data analysis portion. For the elbow 8 out 15 recordings were considered where as for the wrist site 12 out of 15 CNAPs were considered from the right hand of subjects. Prior to stimulating and recording the CNAPs both stimulation sites and recording locations are cleaned using alcohol swabs. To obtain the CNAPs the recording electrodes were attached using Velcro strip soaked in a saline solution to the middle finger

and the stimulation electrodes were placed at wrist and elbow sites. Amplitude of stimulation pulses is increased to as high a level as comfortable for the subject, pulse width used was 0.2ms. The duration of the CNAP recording was 20 ms. The data was collected from the same subject in two sessions one week apart for 5 kHz and 10 kHz.

The experimental data was recorded using Biopac equipment with acknowledge v3.8 application using the averaging mode. The data analysis involved running MATLAB subroutines processing the data collected in order to obtain estimates of CVDs. Plots of the CVD estimates obtained from full CNAPs from elbow and wrist stimulation are presented. For experiments, data was acquired at two sampling rates, a lower rate of 5 kHz and a higher rate of 10 kHz. The two stimulation sites for acquiring the full CNAPs; wrist & elbow were tested and the smoothing techniques were also implemented. The plots for the experimental data include the error bars representing the standard deviation for each of the three estimates; initial estimate (black sold line), smooth CVD estimate (red dashed line) and the filtered CVD estimate (magenta dotted line).

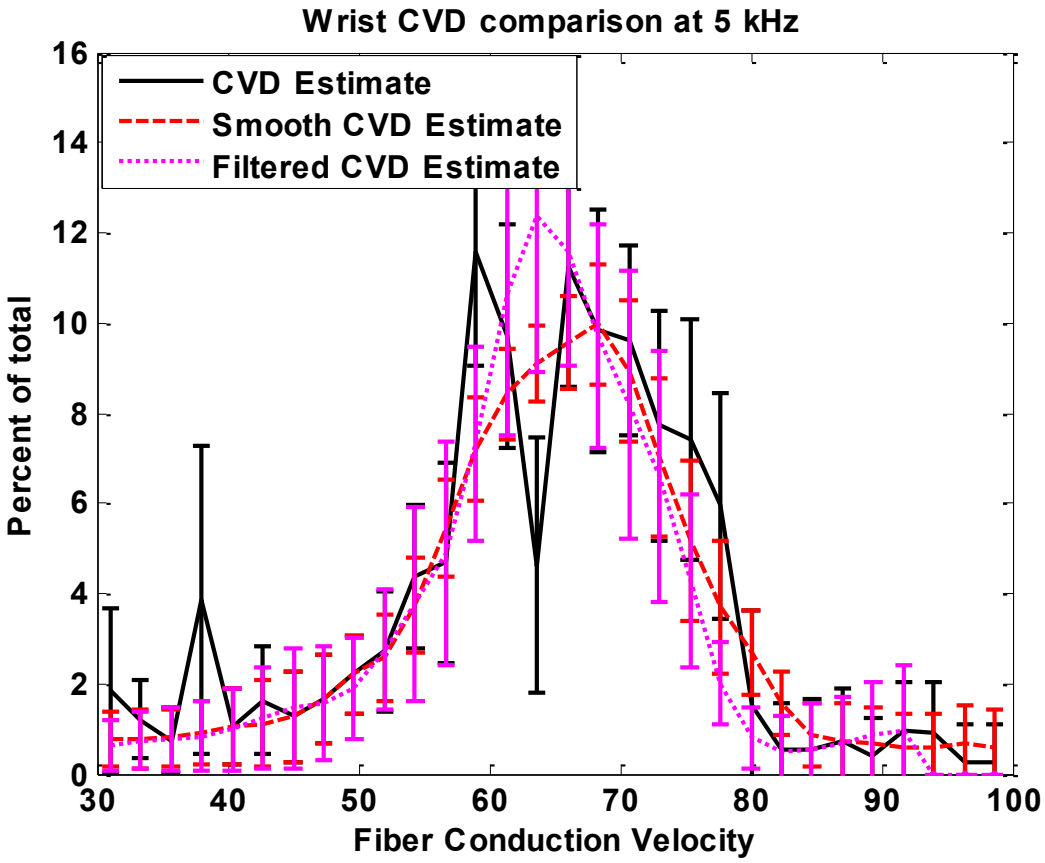

Figure 9 Comparison of CVD estimates of Wrist at 5 kHz

Figure 9 shows CVD estimates obtained for the wrist at a sampling rate of 5 kHz. The full CNAPs collected at 5 kHz during wrist stimulation show an average conduction velocity of 70 m/s with additional peaks present in the range of 55 – 65 m/s. The error bars in the figure represent the standard deviation for that velocity. As simulations suggested the initial CVD estimate is jitterier and improves considerably after applying the smoothing techniques. Though the amplitude of the CVD estimate decreases after applying the smoothing techniques compared to the initial CVD estimate, the estimate is free of any additional peaks and jitter. Looking at the error bars it can be said that the initial CVD has the highest standard deviation of all the three estimates. The values shown in Table 5

corroborate these findings.

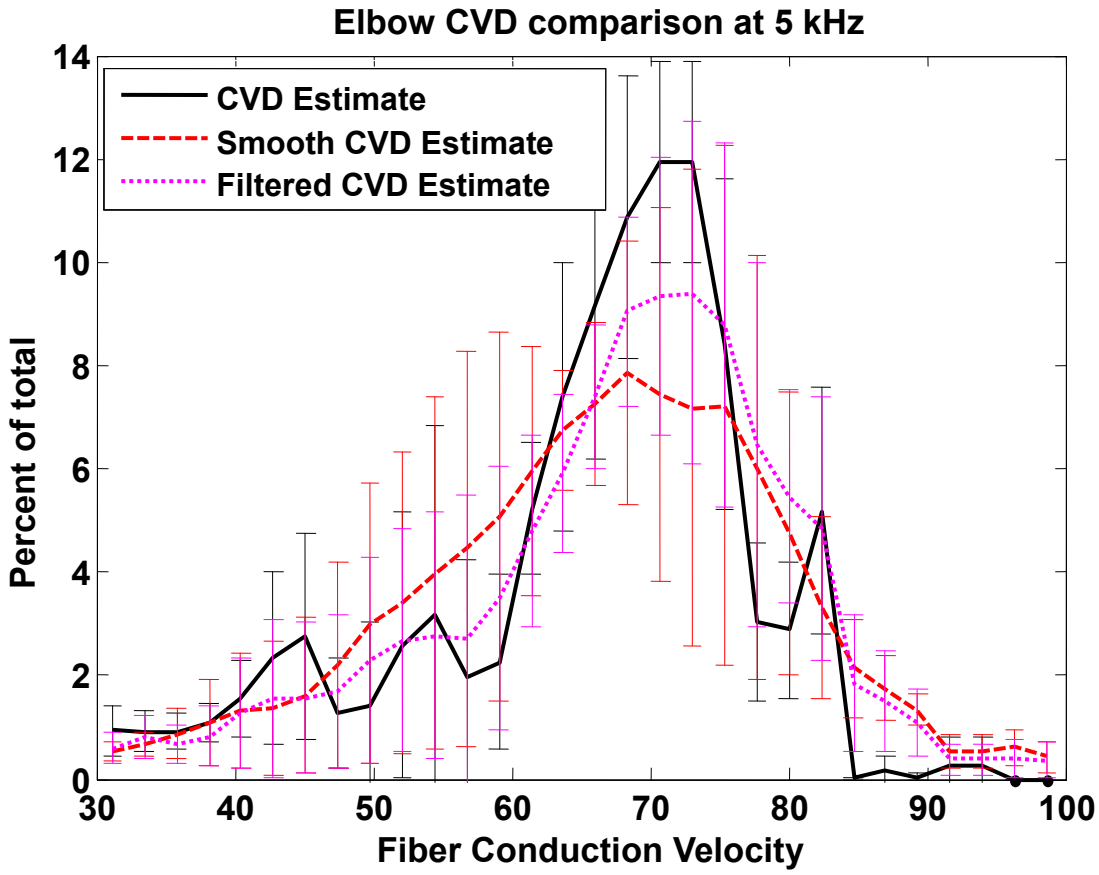

Figure 10 Comparison of CVD estimates of Elbow at 5 kHz.

The full CNAPs for the elbow at 5 kHz were obtained in the same session along with the data collected from the wrist at 5 kHz. Figure 10 shows the CVD estimates obtained from the full CNAPs elicited at the elbow with a sampling rate of 5 kHz. The initial CVD estimate is less jittery compared to the CVD obtained at the wrist for a sampling rate of 5 kHz. With the application of the smoothing techniques the jitteriness in the CVD estimates is reduced. As a measure of performance the standard deviation values have been tabulated.

Table 5 Standard deviation values for the wrist and elbow site at 5 kHz

Sampling rate = 5kHz	Initial CVD	Smooth CVD	Filtered CVD
Wrist	2.4	1.5	1.2
Elbow	2.3	1.6	1.4

The standard deviation was computed for each of the estimates; initial, smooth and the filter CVDs. Table 5 shows the standard deviation values obtained for the elbow and wrist as stimulation sites for the full CNAPs recorded at the middle finger with a sampling rate of 5 kHz. It can be noticed from the table that the standard deviation value is larger for the initial CVD estimate in both cases; wrist and elbow, as also seen in figures 9 and 10. Though the CVD estimates from the wrist and the elbow sites have some jitter in the initial CVD they improve after the smoothing techniques are applied. In the wrist case, the standard deviation value of the smooth CVD is 78% of the standard deviation of the initial CVD while the filtered CVD has a standard deviation that is 70% the standard deviation of the initial CVD estimate.

When the elbow is used as the stimulation site for the full CNAPs the standard deviation is found to be 73% of the initial CVD standard deviation for the smoothing and 64% of the initial CVD standard deviation after the filtering is applied. Although the standard deviation values are higher at the wrist site compared to the elbow it can be noted that the approximate difference in standard deviation reduction after the smoothing techniques are employed between the two sites is only about 5%. The next step was to test the elbow and the wrist sites with an increase in the sampling rate to 10 kHz.

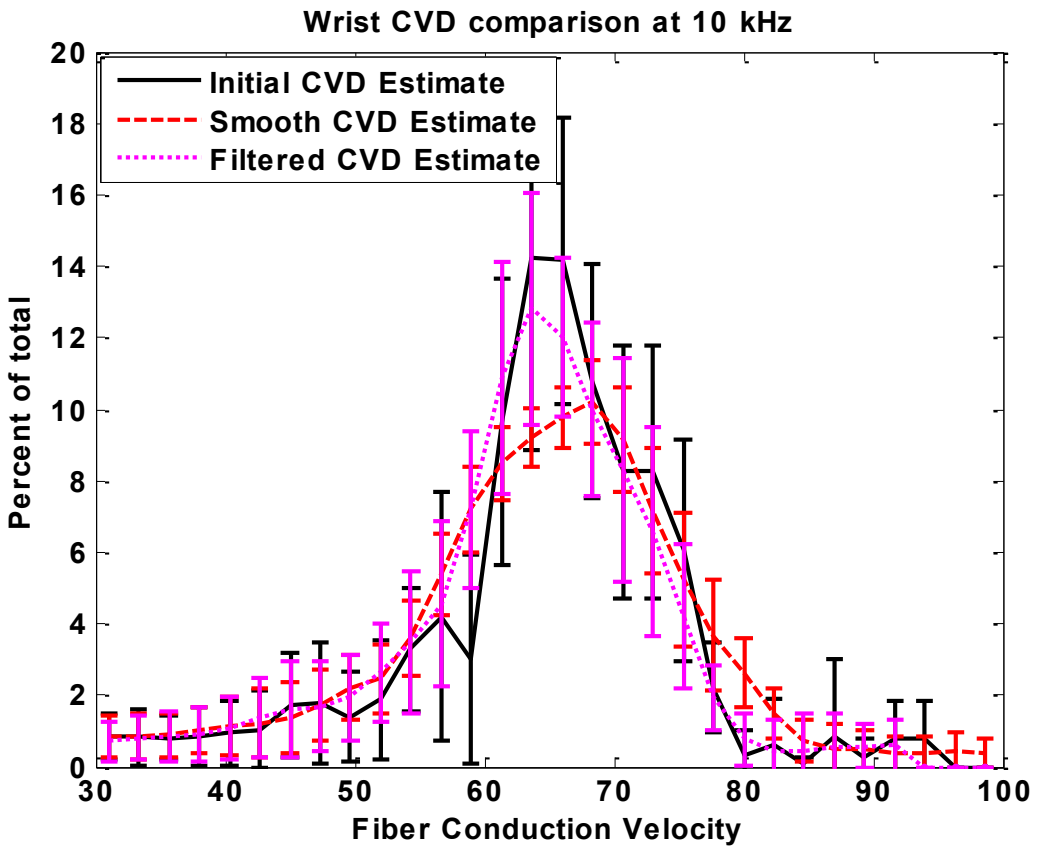

Figure 11 Comparison of CVD estimate of Wrist at 10 kHz

To compare the results obtained at a higher sampling rate of 10 kHz similar conditions were applied; stimulating at the wrist and elbow sites, smoothing and filtering. Figure 11 shows the CVD estimates obtained from the wrist site at 10 kHz. The initial CVD estimate for the wrist site has poor resolution but improves as the smoothing techniques are applied obtaining lower standard deviation values as can be observed from Table 6.

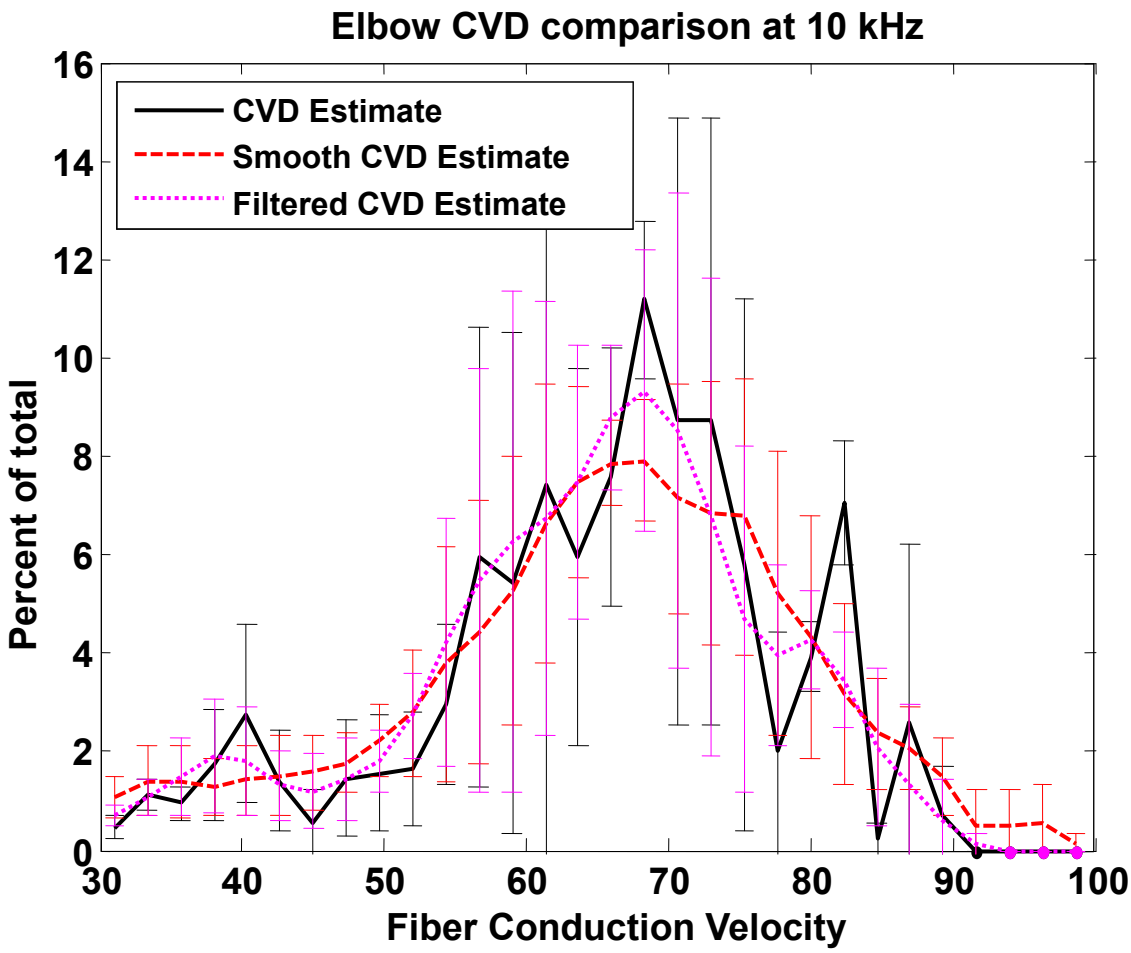

Figure 12 Comparison of CVD estimates of Elbow at 10 kHz.

When the stimulation site is switched to elbow to elicit full CNAPs for a sampling rate of 10 kHz the initial CVD resolution improves compared to the CVD from the wrist. After applying the smoothing techniques the resolution of the CVD estimates improves also as noticed in the earlier cases. To further understand and clearly illustrate the difference between the wrist and elbow CVD estimates the standard deviation values were obtained at 10 kHz, see Table 6.

Table 6 Standard deviation values for the wrist and elbow site at 10 kHz

Sampling rate = 10kHz	Initial CVD	Smooth CVD	Filtered CVD
Wrist	2.0	1.4	1.0
Elbow	2.5	1.8	1.4

A difference among the three estimates for a sampling rate of 10 kHz at different stimulation sites (wrist & elbow) can be noted from Table 6. The standard deviation values obtained for each of the three cases represent the average for CVD sets obtained from the wrist and elbow stimulation for full CNAPs. The initial CVDs for both stimulation sites for 5 and 10 kHz are found to be highest of all three estimates. After the smoothing techniques are employed the standard deviation value was observed to be lower for the wrist site compared to the elbow site.

For the wrist case, the standard deviation value of smooth CVD is 55% of the initial CVD whereas the filtered CVD was found to be 38% of the initial CVD estimate. When the elbow is used as the stimulation site the standard deviation is found to be 72% of the initial CVD for the smoothing and 56% of the initial CVD after the filtering is applied.

3.11 Summary

In simulations the recordings were obtained under two conditions, with and without noise to understand the effect of noise on the CVD estimate. The CVD estimates obtained without noise had a lower PMSE value. However, in experimental recordings the noise component is present and when noise was added to the CNAPs in the simulations it increased the PMSE. When the smoothing techniques were applied to the CVD estimates

the PMSE was considerably lower. The application of the smoothing techniques can be considered an improvement as it produced estimate closer to that of the actual CVD estimate in the simulations and improved the CVD estimate in experimental results with less spikes and jitteriness. Filtering of the CVD estimate shows a promise with smooth edges and sufficiently large amplitude similar to that of the initial CVD estimate. The simulation results showed that with the increase in the sampling rate an improvement can be achieved and further can be accomplished by smoothing techniques. As seen in the simulations, CVD estimates obtained from the full CNAPs elicited from the wrist have a poor resolution compared to those obtained from the full CNAPs elicited from the elbow. However after applying smoothing techniques the estimates have reduced jitteriness and lower PMSE values are obtained compared to the initial CVD estimate.

In the experimental results, the standard deviation reduction at a 5 kHz sampling rate was found to be 22% for the wrist site and 27% for the elbow site after smoothing was employed. For the filtered CVD estimates the standard deviation value at 5 kHz was found to be 30% lower than the initial CVD standard deviation value for the wrist and 36% lower than the initial CVD standard deviation value for the elbow.

At a sampling rate of 10 kHz for the wrist site after smoothing the CVD the standard deviation was 45% lower than the initial CVD standard deviation value and for the elbow site it was found to be 28% lower than the initial CVD estimate. The standard deviation reduction after filtering was employed at 10 kHz sampling rate for the wrist site was found to be 62% lower with respect to the initial CVD standard deviation value and for the elbow site it was found to be 44% lower with respect to the initial CVD standard

deviation value.

It can be concluded from the results obtained that the wrist site offers better CVD estimates and provides a solution for the drawbacks (1) of consistency to innervate the same nerve fibers when stimulating at the elbow site to elicit full CNAPs and (2) recruitment of motor fibers causing limb movement resulting in movement artifacts. The CVDs estimated from the full CNAPs obtained from the wrist site suffer due to the shorter stimulating–recording site distance at a sampling rate of 5 kHz. This problem can be overcome by employing the smoothing techniques. When the sampling rate is increased to 10 kHz in the experiments it improves the CVD estimate and with the application of filtering the resolution problem can be overcome. Another point to be noted here is that due to inconsistency in stimulating at the same site for full CNAP at the elbow the CVD estimates obtained are spread over different intervals.

CHAPTER 4 Impact of Decomposition Errors on EMG Signal Coherence

This chapter provides the reader with an understanding about motor control studies and the effects of errors incurred during decomposition of the recorded EMG data. Many researchers have studied the electrical activity in muscles from different points of view and have found various parameters to observe the motor unit activities, such as common drive, synchrony or common input strength (CIS) and coherency.

As described in chapter 2, in the EMG signal decomposition the signal is decomposed into constituent MUAPTs from which various parameters are revealed. Among these are shapes, amplitude and time duration of the MUAP waveforms that can have different physiological significances. From the point of view of control properties of MUs, the informative parameter is the activation or discharge times of the MUs, since it is known that in addition to recruitment of MUs, the CNS modulates their firing rate in order to regulate the force output.

A MU in a normal muscle does not fire at constant intervals but rather in an irregular manner. Therefore the firing behavior of a MU is best described in statistical terms. Two commonly used statistics to characterize MU firing behavior are the time between two consecutive MU firings, known as the inter-spike interval (ISI) or inter-firing interval (IFI), and the average firing rate computed as the reciprocal of the average IFI. In obtaining a mean firing rate estimate based on the firing times, averaging the IFI over a certain number of firings has been used.

4.1 Decomposition Errors

Misinterpretation of the data or introduction of errors happens all the times let that be due to the faulty equipment or due to human intervention. This chapter discusses the error tolerance of the EMG signal. The firing times are obtained from the MUAPTs, these firing times are then used to introduce the errors. There are three possible types of errors in identifying the firing times: failing to identify a MU firing or false negative (FN), identifying a spurious firing time or false positive (FP) and the combination of missing the correct MU firing time and assigning it to the wrong MU or false negative positive (FNP). Apart from different types of errors different levels of errors are also introduced 1 error per 5 secs, 2 errors per 5 secs, 6 errors per 5 secs, 10 errors per 5 secs and 20 errors per 5 secs. This chapter studies the effect of these errors to assess motor control activity using coherence between pairs of MU firing trains.

4.2 Methods

The automatic decomposition of motor units (MU) often produces errors in recording the actual firing times. MU firing times were available both from automatic decomposition ('a' files) and manually corrected files ('b' files). Manually corrected files were considered the gold standard, *i.e.* error free. For each MU in a contraction three different types of errors were randomly introduced on the 'b' files. Each type of error was introduced at five different rates: 1, 2, 6, 10 and 20 errors / 5 sec and for each case 25 random realizations of the error were created. These firing statistics were then used to build the firing rate curves, from which coherence functions were computed for each MU pair.

Coherence functions were calculated for each pair of firing rate curves as described in Eq. 3. The established method was applied to experimental data obtained during low level 20-30% Maximal voluntary contractions (MVC) of the Deltoid and First Dorsal Interosseous muscles of a subject. Epoch lengths used ranged from 30-60 sec.

To quantify the results obtained with the coherence parameter percent mean square error (PMSE) is used.

$$\text{PMSE} = \frac{mean\left\{(Org.coherence - Avg.coherence)^2\right\}}{max\{(Avg.coherence)^2\}} \text{ x } 100 \quad \textbf{Eq. 3.}$$

Where,

Org.coherence, is the coherence function of the original file, and

Avg.coherence is the average coherence function across 25 error realizations.

4.3 Results and Discussion

Figure 13 shows the coherence functions computed from MU firing trains for the FN type of error in all 5 error rates. It can be observed that there is a decreasing trend on coherence values with the increase in the error rate from 1 error/ 5 sec to 20 errors/ 5 sec, especially for frequencies 0 – 5 Hz, and in general the coherence function departs from its original.

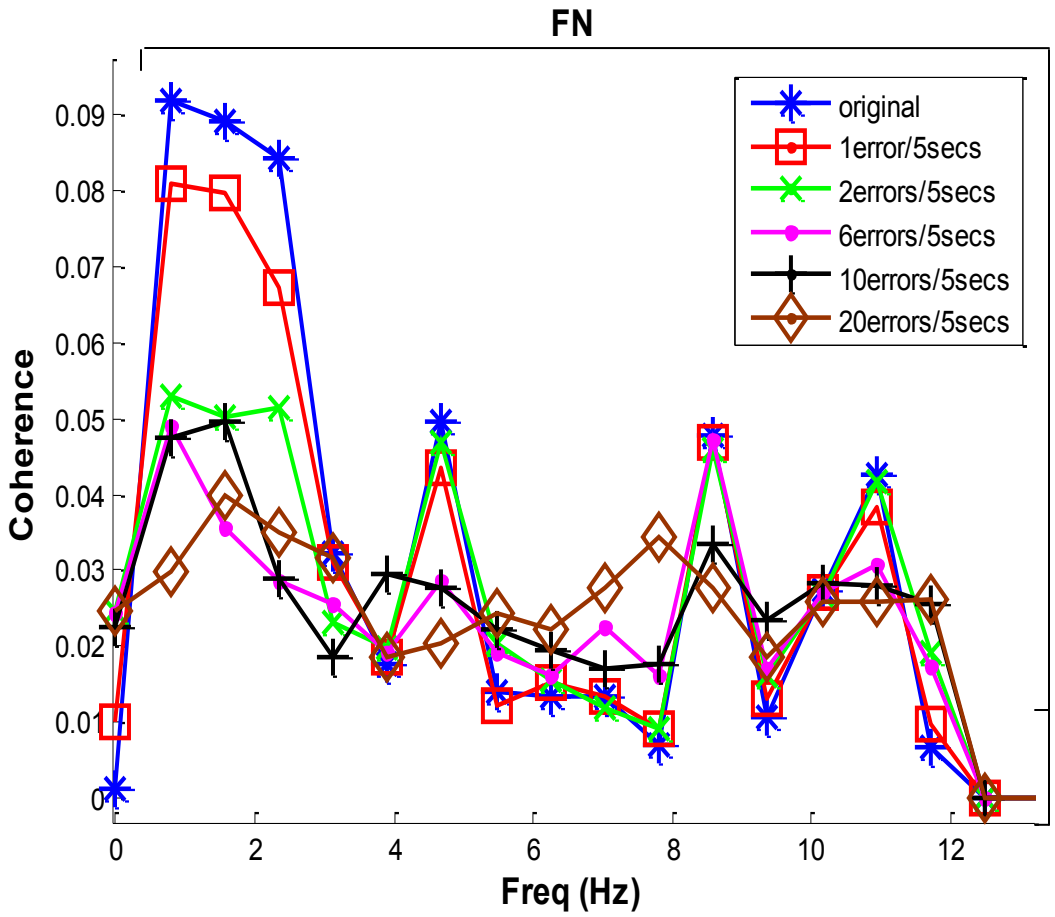

Figure 13 Coherence plots obtained for different error rates in the FN case.

In Figures 13 through 15 the blue curve with a star marker is the original coherence obtained from the manually decomposed 'b' files. The bottom five traces in the figure legend all show the coherence obtained after the FN, FP and FNP errors are introduced at different rates to the MU firing trains.

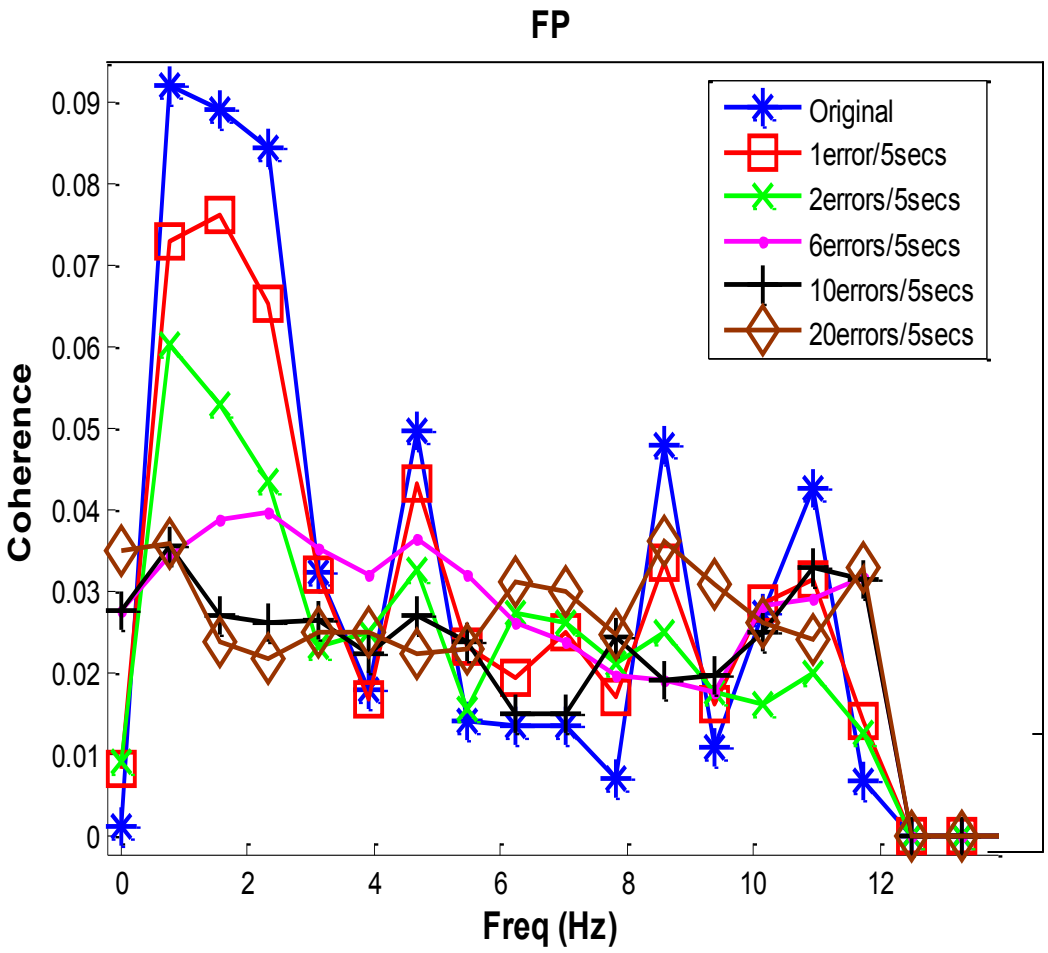

Figure 14 Coherence plots obtained for different error rates in the FP case

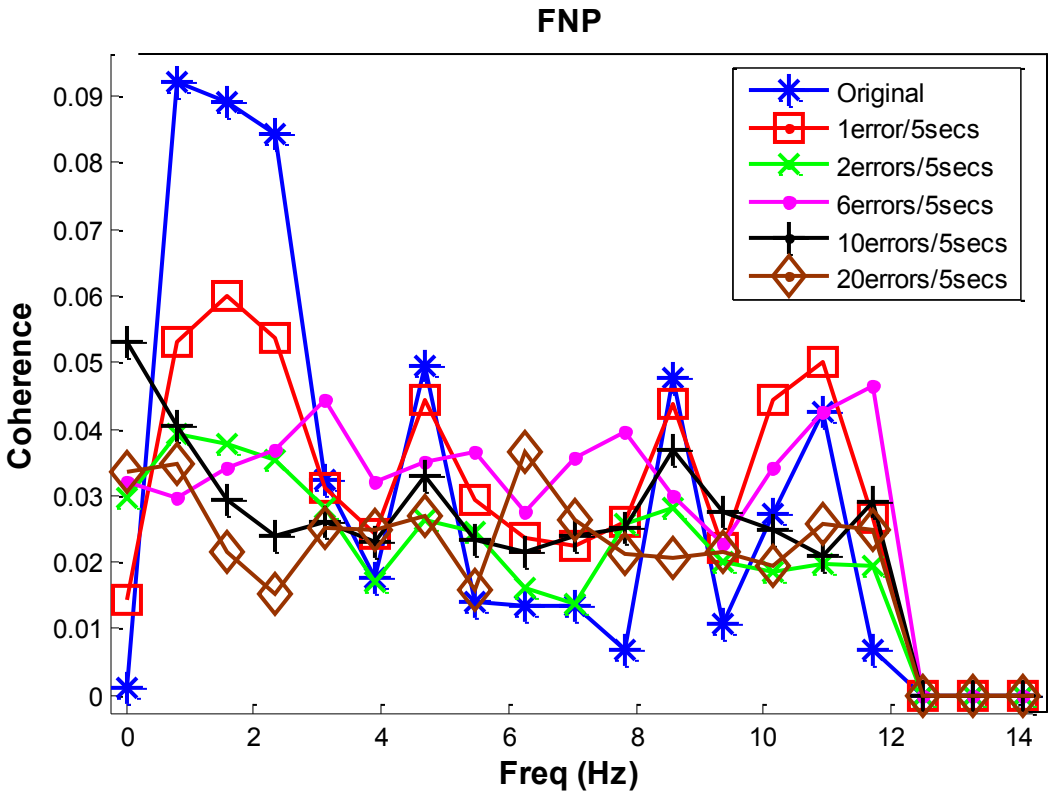

Figure 15 Coherence plots obtained for different error rates in the FNP case

The plots shown in figures 13 through 15 illustrate the 3 error types, FN, FP & FNP. It can be observed that in FP & FNP cases the amplitude of the coherence value is relatively small. However, in presence of FN errors the coherence retains most of its shape while following the decreasing trend of its amplitude as the error rate increases refer figure 13.

As the error rate increases from 1 error/5 sec to 20 errors/5 sec, the PMSE between the coherence curve found for the original manually decomposed b files and the coherence curve found for those files with errors increased. It was observed that the PMSE for the FN type of error remained relatively low compared to the FP and FNP. In other words, the FN type of error is the least detrimental of the three errors as it affects the coherence functions

the least for all error rates. Table 7 shows how much the coherence was affected by the different error rates for all 3 error types. This change is represented in terms of the PMSE.

Table 7 PMSE values for different error rates

Error Type	Error Rate				
	1/5s	**2/5s**	**6/5s**	**10/5s**	**20/5s**
FN	1%	9%	12%	22%	31%
FP	4%	14%	29%	38%	42%
FNP	9%	28%	33%	36%	48%

Table 4-1 presents the percent error in the estimation of the coherence function with respect to the original b file. It can be seen that with an increase in the error rate there is an increase in the PMSE. For the FN type of error the PMSE remains under 15 % up to 6 errors per 5 secs and for the FP the PMSE remains under 15% for up to 2 errors per 5 secs. The PMSE ranges between 25% and 35% when the error rate is 6 errors/ 5 sec for the FP and FNP errors. As the error rate is increased to 10 and 20 errors per 5 secs the PMSE further increases ranging from 30% to 50% and resulting in a significant distortion of the coherence function.

4.4 Summary

The PMSE values decrease for all three error types as a result of increasing error rates from 1 error/5 sec to 20 errors/5 sec. Table 7 shows that the PMSE value for the FN error at a rate of 20 errors/5sec is nearly equal to the PMSE values for the FP and FNP errors at a lower rate of 6 errors/5sec. This indicates that the FN type of error has lesser impact on the coherence compared to that of the FP and FNP types of errors. Hence, for FP and FNP types, 2errors/5sec or higher is significantly detrimental to coherence estimation,

while for the FN type the highest tolerable error rate is somewhere between 2errors/5sec and 6errors/5sec.

Coherence plots were obtained for different error rates in the FN case. There was a small mismatch in the estimation of the coherence for the lower frequencies however for the most part the coherence function estimated in presence of FN errors follows closely the coherence obtained from the original signals. When the error rate is increased up to 10 errors/5 seconds and beyond the coherence function estimated tends to flatten out like the spectrum of white noise as the error level adds randomness and overwhelms the coherence present in the original manually decomposed signals. The coherence functions also flatten for FP & FNP error types, however this occurs at lower error rates in these cases.

CHAPTER 5 Conclusions and Future Work

5.1 Conclusions

One of the main objectives of this thesis was to improve the current diagnostic technique used to diagnose CTS. The improvements were focused on improving the CVD estimate. Three issues were of interest in this study;

i. The assessment of the stimulation site used to elicit the full CNAP for estimating the CVD.
ii. To determine the effect of different sampling rates and
iii. The application of smoothing techniques to improve the CVD estimate.

These issues were analyzed by performing simulations and the results verified with experimental estimates. The simulations and CNAP recordings collected from subjects were processed in MATLAB.

The other part of this thesis was to study the impact of decomposition errors. Different types and levels of errors were introduced to original firing times or the true recording. Three different types of errors are introduced; False negative (FN), False positive (FP) and False negative positive (FNP). Five levels of errors were introduced to 25 realizations which varied from 1error per 5 secs, to 20 errors per 5 secs.

iv. The objective was to study the impact of decomposition errors on the EMG signal coherence. The data obtained was processed in MATLAB.

Chapter 3 discussed in detail the stimulation sites; elbow and wrist along with

different sampling rates, 5 & 20 kHz in simulations and 5 & 10 kHz in the experimental setup. The possibility of improving CVD estimation with the help of smoothing techniques was presented. The filtering has provided CVD estimates with lower PMSE values and closer to the actual CVD estimates with less jitteriness in simulations. A detailed analysis assessing stimulation site, sampling rate and smoothing techniques was discussed and tabulated using percent mean square error and standard deviation as performance indices.

From the experimental results it can be concluded that though the CNAPs obtained at the elbow site offer CVD estimates with lower standard deviation values. The standard deviation values are very close to those obtained for the wrist. Also, the drawbacks encountered when stimulating at the elbow site to elicit full CNAPs such as difficulty in activating the same nerve fibers repeatedly and recruiting motor fibers resulting in movement artifacts can be avoided by selecting the wrist as the stimulation site for recording the full CNAPs. The CVDs estimated from the full CNAPs obtained from the wrist site suffer due to the shorter stimulating–recording site distance at both sampling rates of 5 & 10 kHz. This can be overcome by either smoothing or filtering the initial CVD estimate. Filtering is recommended as it performs more consistently offering lower standard deviation values compared to the initial and smoothed CVD estimates.

Chapter 4 introduces the impact of decomposition errors on the EMG signal coherence. Coherence was used to test the degree at which the original files and the error introduced files are similar; what type of error affects EMG signal coherence and at what level. The method involved addition of errors to the manually corrected or original files of firing times. The coherence was then computed between the two MUAPTs for the original

files as well as the ones with the errors within the same contraction. It was found that false negative (FN) type of errors affected coherence estimates the least. Their influence was tolerable up to an error rate of 6 errors per 5secs. Whereas the FP and FNP types of errors affected the coherence estimates more severely. Their influence is only tolerable for the lowest error rate of a single error per 5 secs.

5.2 Contributions

The contributions made as part of this thesis are as follows:

1. Evaluation of the protocol described by Sundar.S [38] led to improvements in the experimental setup that will help achieve more consistent CVD estimates. Experimental results in agreement with simulations suggest that changing the stimulation site to the wrist allows for easier recording of the full CNAPs and also achieves consistent CVD estimation over repeated trials. As a result, the wrist site was found to be the better choice for stimulation.
2. Some signal information was observed in the spectrum of the full CNAP beyond 2.5 kHz therefore an increase in sampling rate from 5 kHz to 10 kHz was determined to be best suited to obtain a CVD estimate without losing signal information. By implementing the smoothing techniques the problem of CVD resolution posed by the short wrist – finger distance has been compensated allowing more consistent CVD estimation. Lower standard deviation values compared to the initial CVD in experimental results and lower PMSE in the simulations suggested filtering is the more consistent estimate helping compensate the temporal resolution issues of the CVD estimates. It is my understanding that

filtering has not been applied to CVD estimates in previous nerve conduction studies.

3. To the best of my knowledge this thesis is the only work in the field to assess the impact of decomposition errors on EMG signal coherence. The assessment was performed based on different types of errors at different error levels. It was found that the FN type of error for up to 6 errors per 5 seconds is the least detrimental of all the errors introduced. The FP and FNP types of errors were severely affected at the higher error rates. The only acceptable level of error in both the cases was found to be one error per 5 seconds.

5.3 Future work

Current study can be extended to the following in future:

1. Further analysis of the stimulation site along with sampling rate of 10 kHz on larger sample of subjects will provide a better understanding if wrist is the site to be chosen over elbow to elicit full CNAP for CVD estimation.
2. Application of filtering to the CVD estimates give a closer approximation to the actual CVD as shown in simulations with less jitteriness. This filtered estimate can be used to create a CVD template to assess the degree of severity of CTS. A set of pattern classifiers can be built using the artificial neural networks (ANNs) while other pattern recognition techniques can also be explored.
3. Since there is not much work in the study involving assessment of affect of decomposition errors on the EMG signal. A further study of decomposition errors and their affect on EMG signal will be helpful. This can be achieved by comparing

the contractions with equal lengths, with different force levels and with different decomposition algorithms, will provide better insight in understanding the effect of errors and determining the suitable decomposition technique with minimal error or improving the technique based on the outcome.

References

[1] A. Nishimura, T. Ogura, H. Hase, A. Makinodan, T. Hojo, Y. Katsumi, K. Yagi, Y. Mikami and T. Kubo.. A correlative electrophysiologic study of nerve fiber involvement in carpal tunnel syndrome using current perception thresholds. Clin. Neurophysiol. 115(8), pp. 1921-1924, 2004.

[2] A. Nishimura, T. Ogura, H. Hase, A. Makinodan, T. Hojo, Y. Katsumi, K. Yagi, Y. Mikami and T. Kubo. Objective evaluation of sensory function in patients with carpal tunnel syndrome using the current perception threshold. J. Orthop. Sci. 8(5), pp. 625-628, 2003.

[3] S. Sundar, J. A. Gonzalez and C. S. Gilbert. Conduction velocity distribution estimation using the collision technique—Theory and simulation study. Biomedical Signal Processing and Control 3(1), pp. 94, 2008.

[4] N. Dalkilic, B. Yuruten and B. Ilhan. Somatosensory conduction velocity distribution of median nerve middle palmar digital component. Int. J. Neurosci. 114(2), pp. 153-165, 2004.

[5] E. G. T. Liddell and C. S. Sherrington. Recruitment and some other features of reflex inhibition. Proceedings of the Royal Society of London. Series B, Containing Papers of a Biological Character (1905-1934) 97(686), pp. 488-518, 1925.

[6] N. S. D. Barkhaus.P.E. EMG evaluation of the motor unit - electrophysiologic biopsy, Remodeling of the motor unit in neuromuscular disorders. In Lorenzo NY, Lutsep HL (senior eds): eMedicine: Neurology. St. Petersberg, eMedicine Corp, 2001.

[7] B. Mambrito and C. J. De Luca. A technique for the detection, decomposition and analysis of the EMG signal. Electroencephalogr. Clin. Neurophysiol. 58(2), pp. 175-188, 1984.

[8] C. De Luca J., A. Adam, R. Wotiz, L. D. Gilmore and S. H. Nawab. Decomposition of surface EMG signals. J. Neurophysiol. 96(3), pp. 1646-1657, 2006.

[9] D. Stashuk. EMG signal decomposition: How can it be accomplished and used? J. Electromyogr. Kinesiol. 11(3), pp. 151-173, 2001.

[10] G. Morita, Y. X. Tu, Y. Okajima, S. Honda and Y. Tomita. Estimation of the conduction velocity distribution of human sensory nerve fibers. J. Electromyogr. Kinesiol. 12(1), pp. 37-43, 2002.

[11] F. A. Papadopoulou and S. M. Panas. Bispectral de-noising of the compound action potential for estimation of the nerve conduction velocity distribution. Med. Eng. Phys. 21(6-7), pp. 499-505, 1999.

[12] A. T. Barker, B. H. Brown and I. L. Freeston. Determination of the distribution of conduction velocities in human nerve trunks. IEEE Trans. Biomed. Eng. 26(2), pp. 76-81, 1979.

[13] K. L. Cummins, L. J. Dorfman and D. H. Perkel. Nerve fiber conduction-velocity distributions. II. estimation based on two compound action potentials. Electroencephalogr. Clin. Neurophysiol. 46(6), pp. 647-658, 1979.

[14] H. C. Hopf. Untersuchungen über die unterschiede in der leitgeschwindigkeit motorischer nervenfasern beim menschen. J. Neurol. 183(6), pp. 579-588, 1962.

[15] C. L. Lim, H. Lal and C. Yiannikas. The effect of wrist size on the orthodromic median sensory nerve action potential. Muscle Nerve 18(1), pp. 117-119, 1995.

[16] J. Aunon. Signal processing in evoked potential research: Averaging and modeling. Critical Reviews in Bioengineering 5(4), pp. 323-67, 1981.

[17] C. Berthold and M. Rydmark. 2. morphology of normal peripheral axons. The Axon 1pp. 13-49(37), 1995.

[18] E. Eduardo and D. Burke. The optimal recording electrode configuration for compound sensory action potentials. J. Neurol. Neurosurg. Psychiatr. 51(5), pp. 684-687, 1988.

[19] R. W. Gilliatt, I. D. Melville, A. S. Velate and R. G. Willison. A study of normal nerve action potentials using an averaging technique (barrier grid storage tube). J. Neurol. Neurosurg. Psychiatr, 1965.

[20] G. D. Dawson. The relative excitability and conduction velocity of sensory and motor nerve fibres in man. J. Physiol. 131(2), pp. 436-451, 1956.

[21] T. A. Sears, "Action potentials evoked in digital nerves by stimulation of mechanoreceptors in the human finger." J. Physiol. (Lond.), pp. 30-31, 1959.

[22] Buchthal, F, Rosenfalck, A., "Evoked action potentials and conduction velocity in human sensory nerves." Brain Res. , Spl Issue, vol. 3, pp. 1-122, 1966.

[23] D. Goddard. Measurement of nerve conduction--a comparison of orthodromic and antidromic methods. Clin. Rheumatol. 2(2), pp. 169-74, 1983.

[24] C. F. Bolton, "Factors affecting the amplitude of human sensory compound action potential." Amer. Ass. EMG Electrodiagn., pp. 46, 1981.

[25] H. Nodera and R. Kaji. "Chapter 5 principles of stimulation and recording," in Handbook of Clinical Neurophysiology, Jun Kimura, Ed. vol. 7, 2006

[26] W. Tackmann. Comparison of orthodromic and antidromic sensory nerve conduction velocity measurements in the carpal tunnel syndrome. J. Neurol. 224(4), pp. 257-66, 1981.

[27] C. Gondran. Noise of surface bio-potential electrodes based on NASICON ceramic and ag-AgCl. Medical Biological Engineering Computing 34(6), pp. 460-6, 1996.

[28] Gondran C., Siebert E., Yacoub S. and Novakove. Dry electrode based on nasicon ceramic for surface biopotential measurements : Skin-electrode impedance and noise, 1995

[29] M. Fernandez and R. Pallas-Areny. Ag-AgC1 electrode noise in high resolution ECG measurements. Biomedical Instrumentation and Technology 34pp. 125-130, 2000.

[30] D. T. Godin, P. A. Parker and R. N. Scott. Noise characteristics of stainless-steel surface electrodes. Med. Biol. Eng. Comput. 29(6), pp. 585-590, 1991.

[31] L. A. Geddes. Electrodes and the Measurement of Bioelectric Events, Wiley-Interscience, a division of John Wiley, 1972.

[32] E. Huigen, A. Peper and C. A. Grimbergen. Investigation into the origin of the noise of surface electrodes. Med. Biol. Eng. Comput. 40(3), pp. 332-338, 2002.

[33] S. H. Nawab, R. P. Wotiz and C. J. De Luca. Decomposition of indwelling EMG signals. J. Appl. Physiol. 105(2), pp. 700-710, 2008.

[34] S. Ahmed. EMG signal decomposition using wavelet transformation with respect to different wavelet and a comparative study. ACM International Conference Proceeding Series 403pp. 730-735, 2009.

[35] D. Tam. Real-time estimation of predictive firing rate. Neurocomputing 52pp. 637, 2003.

[36] C. J. De Luca and Z. Erim. Common drive of motor units in regulation of muscle force. Trends Neurosci. 17(7), pp. 299-305, 1994.

[37] N. Saskia Kathi, "Coherence of human EEG Signals during crossmodal integration of natural stimuli," PICS, vol. 9, 2006.

[38] S. Sundar, Selective Stimulation of Nerve Fibers for Detecting the Severity of Carpal Tunnel Syndrome, Thesis Report, Dept. of Electrical and Computer Engineering, Dalhousie University, 2005.

APPENDIX A – FIGURES

Simulation results obtained at different sampling rates for full CNAPs from wrist and elbow

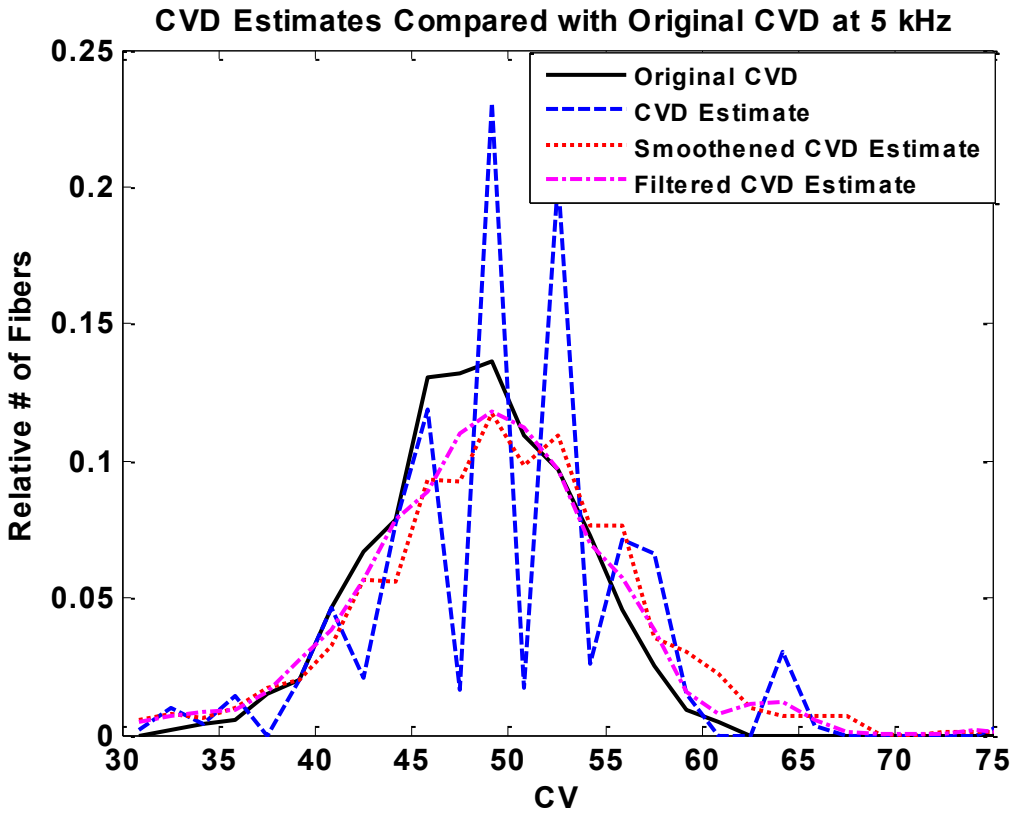

Figure A 1 CVD estimates comparison at a sampling rate of 5 kHz for wrist

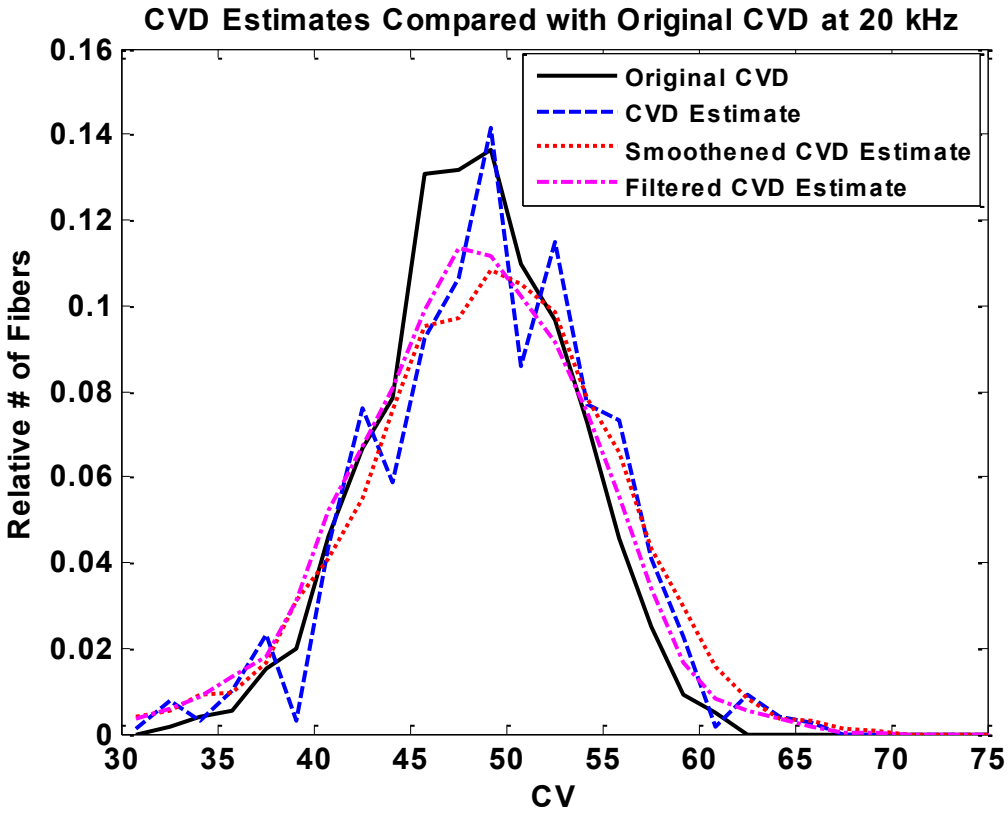

Figure A 2 CVD estimates comparison at a sampling rate of 20 kHz for wrist

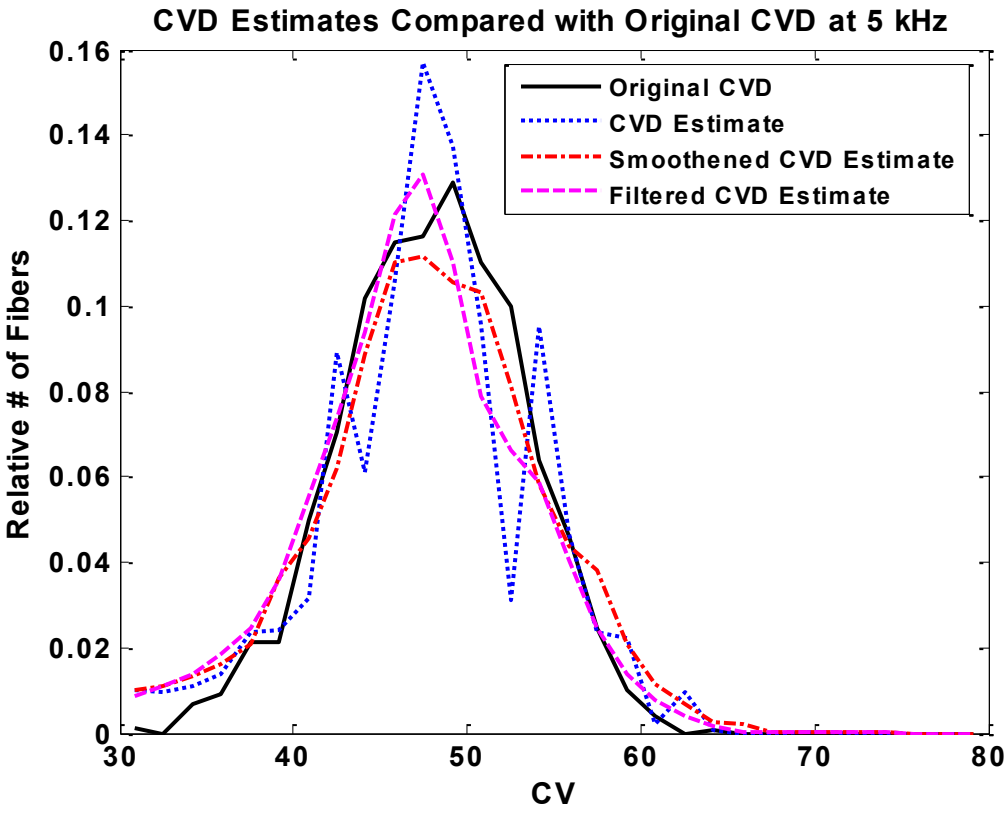

Figure A 3 CVD estimates comparison at a sampling rate of 5 kHz for elbow

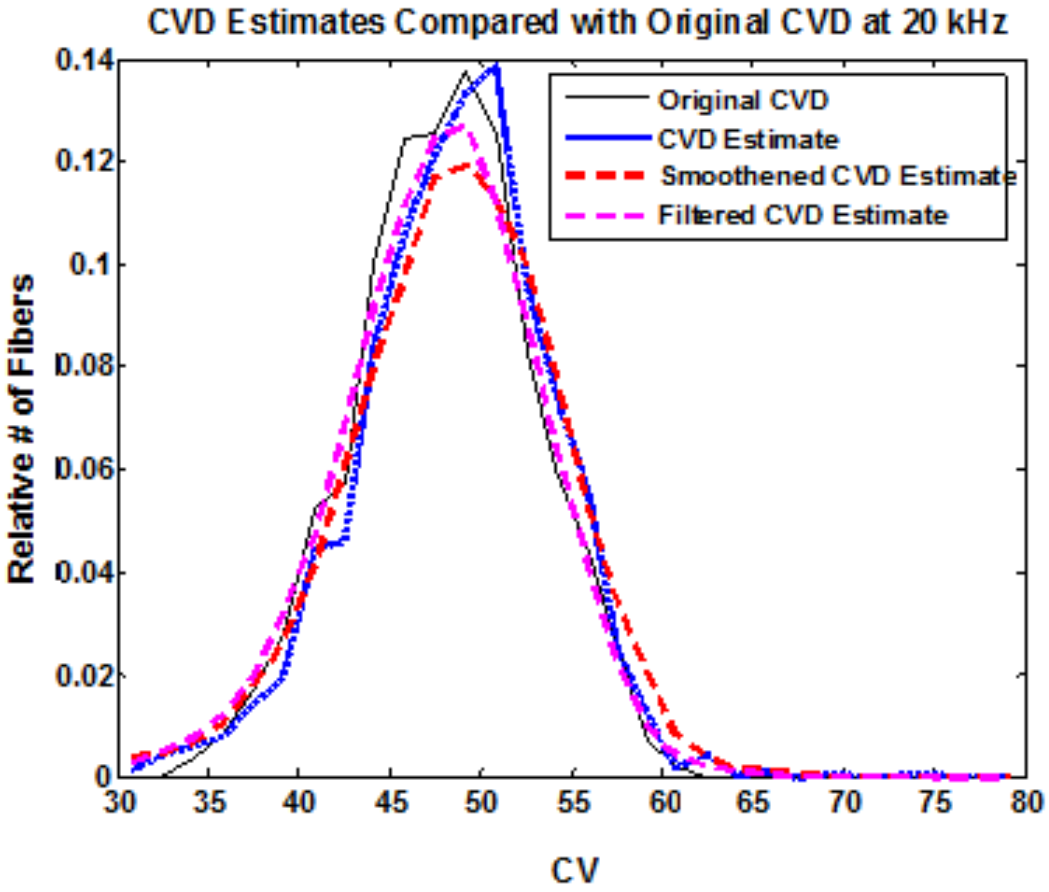

Figure A 4 CVD estimates comparison at a sampling rate of 20 kHz for elbow